Vol. 48, No. 2 (2026) 392-417, DOI: 10.24874/ti.2157.03.26.05

Tribology in Industry

www.tribology.rs

RESEARCH

Predictive Modeling and Parametric Analysis of Three-Body Abrasive Wear in Hybrid CNF-GF/PPS Nanocomposites

Y.C. Arun[a], R. Ravishankar[a], B. Suresha[a,*], V.G. Pradeep Kumar[a], M.N. Thejaswini[a], V.M. Mahesh[a]

[a]*Department of Mechanical Engineering, Sri Jayachamarajendra College of Engineering, JSS Science and Technology University, Mysuru -570006, Karnataka, India.*

Keywords:

Polyphenylene sulfide hybrid nanocomposites
Carbon nanofibers
Three-body abrasive wear
Box–Behnken design
ANOVA
Worn surface morphology

* Corresponding authors:

B. Suresha
E-mail: sureshab@jssstuniv.in

Received: 19 March 2026
Revised: 24 April 2026
Accepted: 25 May 2026

A B S T R A C T

Three-body abrasive wear is a major degradation mechanism in fiber-reinforced thermoplastic composites used in demanding automotive and aircraft components. Under abrasive wear circumstances, this work examines the wear performance and predictive modeling of carbon nanofiber (CNF) filled short glass fiber/polyphenylene sulfide (GF/PPS) hybrid nanocomposites. To assess the impact of CNF content on microstructure, density, hardness, interlaminar shear strength, and abrasive wear behavior, nanocomposites with varying CNF levels (0–1 wt%) were produced using extrusion and injection molding. The microstructural data are in support of the integration of CNF to strengthen the fiber/matrix interface and boost the load transmission and crack-bridging features by the formation of a well-dispersed reinforcing structure at the nanoscale. Density study revealed that excessive loading led to agglomeration and increased porosity whereas moderate CNF addition (0.6 and 0.8 wt%) reduced void content and enhanced packing effectiveness. The baseline composite had a Barcol hardness of 44.2, which improved to 54.3 with 0.8 wt% CNF. Box–Behnken design was planned for the abrasive wear trials considering load, abrading distance and filler content and response surface methodology was used for the analysis and optimization. Statistical analysis indicates that load and CNF content have a significant impact on wear loss. Additionally, compared to the GF/PPS composite, the addition of 0.8 wt% CNFs greatly increased the abrasion resistance of baseline composites, as evidenced by the development of very small and shallow grooves, smoother worn surfaces, and decreased wear loss. ANOVA and response surface analysis revealed that CNF content and applied load were the most significant parameters determining wear loss, while the proposed model exhibited good predictive accuracy (R^2=86.87%, adjusted R^2=83.29%). A dependable framework for creating wear-resistant GF/PPS hybrid nanocomposites for cutting-edge tribological applications is provided by the established prediction model.

© 2026 Published by Faculty of Engineering

1. INTRODUCTION

Glass fiber-reinforced thermoplastic composites are widely used in industrial, automotive, and aerospace applications due to their exceptional chemical resistance and high strength-to-weight ratio. The main drawback of fiber-reinforced polymer composites is their poor resistance to abrasive wear in three-body contact situations, despite their extensive use in structural and tribological applications. Trapped hard particles between the mating surfaces aggravate micro-cutting, ploughing, and surface fatigue, especially in hazy or polluted operating circumstances. This results in faster material degradation, early component failure, and shorter service life [1,2]. The use of carbon-based nanofillers has proven to be a successful solution to this problem since they improve interfacial adhesion, load transfer efficiency, crack-arrest capability, and surface hardness by forming a strong reinforcing interphase between the fibers and polymer matrix [3,4]. These improvements are widely sought after for demanding applications in the manufacturing, transportation, and energy sectors, where wear reliability and long-term durability are crucial. In this regard, the current study explores the incorporation of carbon nanofibers (CNFs) into the composite system and uses Box-Behnken Design (BBD)-based Response Surface Methodology (RSM) to maximize the three-body abrasive wear performance, thereby aiding in the development of high-performance and sustainable advanced composite materials.

Abrasive wear, prevalent in polymer composites, manifests as two-body (hard asperities fracturing softer surfaces) or three-body (loose particles inducing ploughing and debris formation) [5]. Wear loss correlates with material hardness, particle geometry, load, and distance; Rabinowicz modeled it as $V = \frac{NL\tan\theta}{\pi H}$ (θ: cone angle, H: hardness), while others proposed stages involving deformation, friction, and fracture, yielding $V = \frac{c\mu N}{H\epsilon\sigma}$ (μ: friction coefficient, ε: strain-to-fracture, σ: tensile strength) [6,7]. In composites, relationships vary; elastomers exhibit complex ridge formation from frictional heating [8].

The complex phenomena of polymer wear are influenced by a number of factors, including material composition, geometry, surface features, mechanical properties, crystallinity, glass transition temperature, and molecule orientation [9–12]. Operating factors including applied load, velocity, abrading distance, temperature, and the prevailing wear-mode also have a significant impact. Recent nanoscale research has shown that linked stress–temperature effects govern atomic attrition and viscoelastic deformation mechanisms, even though processing-induced orientation can significantly alter crystallinity and abrasion resistance in advanced polymers. Additionally, these characteristics can be effectively adjusted by surface-modified nanofillers, which improves the polymer composites' wear resistance and durability [13].

Through the use of statistical modeling techniques and optimal reinforcing strategies, recent research on fiber and particulate-reinforced thermoplastic composites has demonstrated significant increases in abrasive wear resistance [14,15]. Because of increased filler dispersion and stable transfer film development, carbon fiber (CF) composites treated with fluoropolymer additives demonstrated reduced friction and improved wear resistance at low filler percentages (<10 wt%) in polyphenylene sulfide (PPS)-based systems [14]. Similarly, due to improved interfacial bonding and heat dissipation, PPS composites with silane-treated CF and graphene oxide showed a 175% increase in thermal conductivity, while the friction coefficient dropped from 0.236 to 0.176 and the specific wear rate decreased from 1200 to 300 × 10^{-1} mm^3/N·m [15].

For natural fiber hybrid systems, Sathiyamurthy et al. demonstrated that NaOH treatment significantly affected the specific wear rate and coefficient of friction of paddy straw–pineapple leaf fiber/polyester composites [16]. Design of Experiments (DOE), ANOVA, quadratic models, and Artificial Neural Network (ANN) predictions revealed that treatment duration and concentration were the most important factors for wear optimization. Similarly, Srinivas et al. found that two-body abrasive wear in CF/polyamide blends was considerably reduced by silane-treated graphene and silica nanofillers (up to 3 wt%), with the best hybrid loading of 1.5 wt% each providing the greatest benefit through improved filler–matrix adhesion [17].

Based on Sahin et al.'s modeling experiments, the most significant factor (33.55%) based on RSM–Box–Behnken analysis was the volumetric wear rate of polyamides, which rose with load and sliding speed but dropped with higher tensile strength [18]. Similarly, Sagbas et al. analyzed polyoxymethylene abrasive wear using central composite design inside RSM and shown that both RSM and neural network models successfully predicted wear behavior under various load and sliding distance conditions [19].

The importance of optimization strategies and reinforcement design in enhancing the abrasive wear performance of polymer and hybrid composites has been further demonstrated by recent studies [20–24]. For PTFE matrix composites, Ibrahim et al. used Taguchi–grey relational analysis and found that grit size was the most important factor (94.56%), with optimal circumstances producing a 52% improvement in grey relational grade [20]. Using pin-on-plate and slurry tests, Muhandes et al. investigated engineering plastics (PA, UHMW-PE) and PLA/hemp biocomposites under abrasive conditions, demonstrating that both system variables and intrinsic material properties strongly govern abrasion sensitivity relevant to agricultural machinery applications [21]. Sliding distance had the most impact, followed by load, composition, and abrasive size. Kumar et al. fabricated basalt fiber/marble dust-filled epoxy hybrids and reported optimal mechanical, thermo-mechanical, and three-body abrasive wear resistance at 5 wt% marble dust [22]. For multi-objective optimization of Al-Zn-Mg-Cu composites under two-body abrasion, Saradar et al. combined artificial neural networks (ANN) and genetic algorithms. They found that the main variables influencing wear rate, friction coefficient, and surface roughness were reinforcement content and abrasive size [23]. Similar to this, Savas et al. demonstrated that excessive fiber rigidity in HDPE composites can lower abrasive wear resistance due to the effects of repeated ploughing; on the other hand, basalt fiber composites with polyethylene grafted maleic anhydride compatibilizer performed better because of improved fiber–matrix adhesion, balanced stiffness, and hardness [24].

Several DoE techniques, including Taguchi, RSM, factorial design, and regression analysis, have been used to optimize composite formulations and processing parameters, as Table 1 summarizes. Fly ash, graphene, carbon nanotubes (CNTs), multiwalled carbon nanotubes (MWCNTs), and graphene nanoplatelets (GNPs) are examples of carbon-based nanofillers that have greatly enhanced the mechanical performance, wear resistance, surface hardness, and lubrication properties of polymer composites while lowering wear rate under ideal filler loading and processing conditions [25-30].

Table 1. Nanofiller composites optimized for wear and mechanical performance.

Composites	Nanofillers	DoE approach	Key findings	Ref.
CF / epoxy	Graphite	Taguchi and Regression	-Wear loss increased with higher applied loads, sliding distances, and weight fractions of graphite filler.	[25]
Hemp/bamboo-epoxy	Microcrystalline cellulose (MCC)	RSM	-High accuracy (R^2 = 95.84 to 97.06%). -Grit and abrading distance dominate wear loss. -MCC controls friction; MCC + grit affects roughness.	[26]
PC / PBT / GF	GNPs	RSM / ML	-18% increase in surface hardness due to GNP shielding effect. -Deflected abrasive sand grains because of high aspect ratio of GNPs. -GNP loading identified as the key factor for wear control.	[27]
Himalayan agave fiber/ polyester	Fly ash	Taguchi's method	-Taguchi L9 optimization applied. -Optimal conditions: 15 wt.% fiber, 10 N load, 15 wt.% fly-ash, 100 rpm. -Lowest abrasive wear rate achieved.	[28]
Hybrid Fiber / PE	Carbon Fillers	Taguchi	-35% higher wear resistance by filling micro-voids. -Hybrid fillers created a denser composite. -Reduced abrasive furrow depth in 3BAW tests.	[29]
CNT-graphene/rubber	CNTs and graphene	RSM and CCD	-High model accuracy: R^2 = 0.9634 (sensitivity), R^2 = 0.9115 (compression modulus). -CNT 1.1 graphene 1.0 g, mixing time 15 min, curing temperature 68.6 °C. -Sensitivity 0.385 kPa^{-1} and compressive modulus 601.567 kPa.	[30]

A lot of research has been done on optimization of tribological performance of fiber-reinforced polymer composites (FRPCs) using DoE approaches like Taguchi, RSM, and ANN but most of the studies have mainly focused on dry sliding or two-body abrasive wear by using conventional microfillers. For example, recent studies have reported wear prediction of steel-embedded glass/epoxy hybrid composites under dry sliding conditions using RSM [31], optimization of abrasive wear in CF/epoxy system through Taguchi methods [32] and ANN-based prediction of mechanical and tribological responses of composite materials under different processing conditions [33]. Similarly, hybrid thermoplastic composites with graphene/CNT fillers were investigated mostly for friction reduction and adhesive wear resistance but not for three-body abrasive wear [34,35]. The research shows the rising importance of predictive modeling, but there is no systematic examination on the three-body abrasive wear (3BAW) behavior of modern thermoplastic nanocomposites.

Therefore, a considerable research gap exists in the comprehension and reliable prediction of 3BAW behavior of CNF modified short glass fiber reinforced polyphenylene sulfide (GF/PPS) composites, especially under actual silica sand abrasion circumstances. As far as the authors are aware, no thorough study exists that integrates the RSM-BBD framework for modeling and optimizing the 3BAW response of hybrid CNF filled GF/PPS nanocomposites. In the present work, Box-Behnken Design (BBD) was used as an efficient statistical design technique to systematically examine the influence of the major operating factors including applied load, abrading distance and CNF content on the wear loss. The selected design structure allows the construction of a reliable quadratic regression model, the analysis of the interactions between the factors and the optimization of the response with a small number of experimental tests, reducing the cost and experimental complexity, and increasing the predictive capacity.

2. MATERIALS AND METHODS

2.1 Materials

The matrix material employed was polyphenylene sulfide (PPS) with good mechanical strength, thermal stability and chemical resistance. It is a semi-crystalline thermoplastic with inherent flame resistance, strong dimensional stability and low moisture absorption. Also, it maintains mechanical integrity at high temperatures and has good resistance to oxidation, solvents, fuels, and corrosive media. Commercial PPS granules were procured from Padmini Innovative Marketing Solutions Pvt Ltd, Mumbai, India. Table 2 gives the essential characteristics.

Table 2. The main characteristics of PPS for hybrid nanocomposites [Manufacture's/ literature].

Property (unit)	Value (Typical Range)	Implication
Density (g/cm^3)	1.34 – 1.36	Enables high-temperature processing
Melting Temperature (Tm) (°C)	280 – 290	Lightweight thermoplastic for structural composites
Glass transition temperature (Tg) (°C)	85 – 90	Indicates thermal stability under moderate temperatures
Tensile strength (MPa)	70 – 90	Good load-bearing capability
Tensile modulus (GPa)	3.0 – 4.0	High stiffness for thermoplastic matrices
Heat deflection temperature (°C)	240 – 260	Maintains shape under high thermal load
Coefficient of thermal expansion (1/°C)	40 – 55 ×10^{-6}	Excellent dimensional stability

In PPS composites, a sterically hindered phenolic antioxidant called pentaerythritol tetrakis [3-(3,5-di-tert-butyl-4-hydroxyphenyl) propionate] (PETBP, CAS No. 6683-19-8) was employed. By scavenging free radicals during melt processing, it improves mechanical and thermal stability and lessens thermo-oxidative deterioration.

The main reinforcement of PPS composites was short glass fibers (GFs), which were chosen because of their low cost, ease of manufacturing, and favourable mechanical characteristics. During melt processing, the GFs (length 6 mm, diameter 13 μm) offer a high aspect ratio for effective stress transfer and consistent dispersion. The fibers were purchased from Fine Organics in Mumbai, India, to ensure their compatibility with the PPS matrix and consistent quality. Table 3 lists the chemical composition of the E-glass fibers.

Table 3. Composition of E-glass fibers.

Constituent	SiO_2	Al_2O_3	TiO_2	B_2O_3	CaO	MgO	NaO_3	K_2O
Composition (wt%)	52-56	12-15	0.2	4-6	21-23	0.4-4	0-1	trace

Carbon nanofibers (CNFs) were used as secondary nanoscale reinforcement to enhance the mechanical, and interfacial properties of PPS-based hybrid composites. The CNFs (diameter 30–45 nm, length >80 μm) were supplied by Aritech Chemazone Pvt Ltd., India, and their key properties are listed in Table 4.

Table 4. Important properties of CNFs [Manufacture's / literature].

Property (unit)	Typical Value / Range	Significance in PMCs
Aspect ratio (L/D)	>1778	High aspect ratio for effective stress transfer
Specific surface area (g/m^2)	20-200	Promotes strong interfacial interactions
Density (g/cm^3)	1.8 – 2.1	Lightweight compared to conventional fillers
Tensile Strength (GPa)	2-7	Improves composite strength
Tensile Modulus (GPa)	200-600	Significantly enhances stiffness
Thermal stability (°C)	>600	Suitable for high-temperature PPS processing

The CNFs, GFs, and PPS granules utilized in this research work are depicted in Figure 1(a), (b), and (c), respectively. SEM pictures (Fig. 2) reveal entangled, tubular CNFs that have a typical vapour-grown fibrous shape. They have diameters of 100–200 nm and lengths of several microns. In polymer matrices, this high aspect-ratio structure facilitates efficient load transfer and wear resistance. 95.8 wt% carbon and 4.2 wt% oxygen is shown by EDAX analysis (Fig. 3), indicating high purity with a little amount of surface oxidation appropriate for reinforcing nanocomposite.

(a) (b) (c)

Fig. 1. Photographs of (a) PPS, (b) SGFs, (c) CNFs.

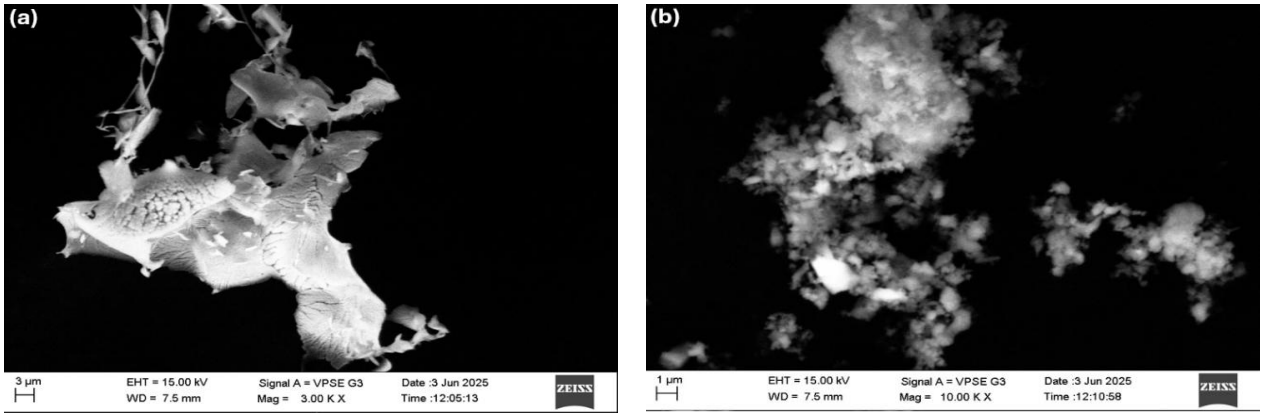

Fig. 2. Microstructure of CNFs: (a) 10 kX, (b) 15 kX.

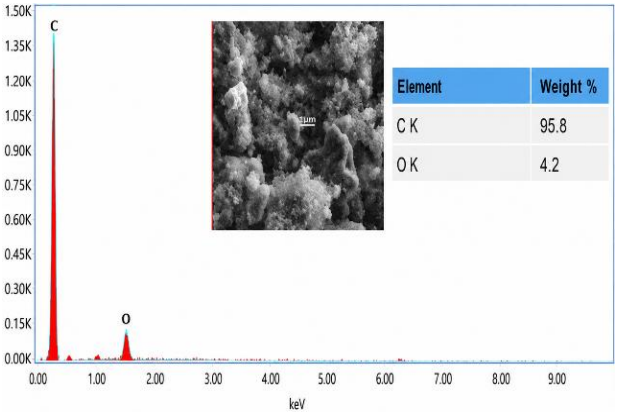

Fig. 3. Energy-dispersive X-ray spectroscopy of CNFs.

2.2 Fabrication of PPS based hybrid nanocomposites

The fabrication route of the hybrid PPS nanocomposites was illustrated in Figure 4 by co-rotating twin-screw extrusion followed by injection molding (Sundaram Polymers, Nanjangud, Karnataka, India). Compounding was done in a Krauss Maffei Berstorff ZE25A twin-screw extruder (screw diameter 25 mm, L/D ratio 44:1). PPS pellets, CNFs, GFs and antioxidant/stabilizer additives were dried at 120–130 °C for 6 h to remove moisture prior to processing. PPS, antioxidant, and CNFs were fed into the extruder throat. Short glass fibers were added by a side feeder at barrel zone 6 to reduce fiber breaking during compounding.

Before compounding, dry PPS pellets were manually premixed with 40 wt% GFs, 0 to 1 wt% CNFs, and stabilizer. Depending on the composite formulation, a co-rotating twin-screw extruder with a throughput of 30 kg h^{-1} and screw speeds of 400–500 rpm was used for melt compounding (Table 5). Short glass fibers were added via a side feeder at the specified barrel zone in order to reduce fiber attrition. Die temperatures were regulated between 340 and 347 °C, while the barrel temperature profile was kept between 78 and 80 °C at the throat zone and 345 and 349 °C next to the die (Table 5). Before injection molding, the extrudates were pelletized and predried for two hours at 120 °C. The set and actual twin-screw extrusion processing parameters recorded throughout the compounding of CNF filled GF/PPS hybrid nanocomposite samples (C0–C5) are shown in Table 5.

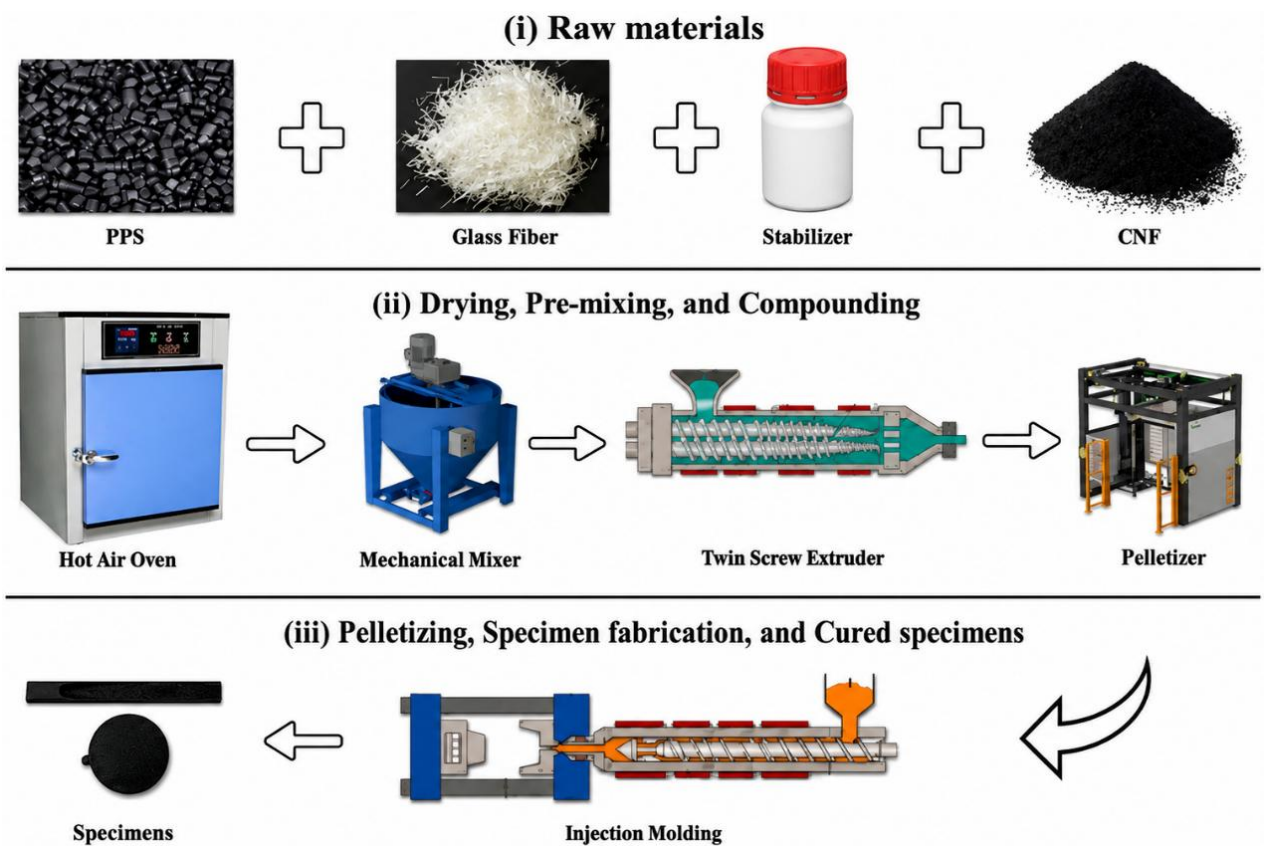

Fig. 4. Fabrication of CNF filled GF/PPS hybrid nanocomposites through extrusion and injection molding.

Table 5. Extrusion parameters for CNF filled GF/PPS hybrid nanocomposite samples (C0-C5).

S No.	Process parameters	Set values	Units	Observed values for composite samples					
				C0	C1	C2	C3	C4	C5
1.	Throughput	30	kgs/h	30	30	30	30	30	30
2.	Screw speed	500	rpm	500	500	500	500	400	400
3.	Barrel temperature Zone 1 (Throat)	80	°C	78	79	78	77	78	78
4.	Barrel temperature Zone 2	330	°C	330	330	330	330	330	330
5.	Barrel temperature Zone 3	330	°C	330	330	331	330	330	331
6.	Barrel temperature Zone 4	330	°C	330	331	331	331	329	330
7.	Barrel temperature Zone 5	300	°C	310	310	309	308	300	303
8.	Barrel temperature Zone 6	320	°C	330	330	330	330	330	331
9.	Barrel temperature Zone 7	330	°C	337	336	335	334	330	331
10.	Barrel temperature Zone 8	330	°C	331	332	333	332	334	333
11.	Barrel temperature Zone 9	345	°C	347	346	345	346	349	346
12.	Die temperature DA	345	°C	347	346	347	346	345	346
13.	Die temperature DH	340	°C	340	340	340	341	340	342

A Milacron Nova Servo 50 injection molding machine with a 22 mm screw diameter and an L/D ratio of 21.9:1 was used to mold test specimens (Table 6). For all composite formulations, the barrel temperature profile was kept between 295 and 296 °C in Zone 4 and 326 and 329 °C at the nozzle (Zone 1). The actual injection and holding pressures were kept at roughly 69 bar and 66 bar, respectively, while a clamp force of 47 tonnes and an injection speed of 160 mm s^{-1} were used. With a screw speed of 200 rpm and a back pressure of 1 bar, the holding, cooling, and cycle times were 5 s, 20 s, and 38–40 s, respectively. Prior to characterization, the specimens were conditioned for 48 hours at 23 ± 2 °C and 50 ± 5% relative humidity after molding.

Table 6. Injection molding parameters of CNF filled GF/PPS hybrid nanocomposite samples (C0-C5).

S No.	Process parameters	Set values	Units	Observed values for composite samples					
				C0	C1	C2	C3	C4	C5
1.	Barrel temperature Zone 1 (Nozzle)	330	°C	328	329	326	328	327	328
2.	Barrel temperature Zone 2	320	°C	321	322	320	322	320	321
3.	Barrel temperature Zone 3	310	°C	312	310	311	310	312	310
4.	Barrel temperature Zone 4	300	°C	295	296	295	295	296	295
5.	Clamp force	45	Ton	47	47	47	47	47	47
6.	Injection speed	160	mm/sec	160	160	160	160	160	160
7.	Injection pressure	150	bar	69	69	69	69	69	69
8.	Injection time	4	sec	4	4	4	4	4	4
9.	Hold speed	20	mm/sec	20	20	20	20	20	20
10.	Hold pressure	85	bar	66	66	66	66	66	66
11.	Hold time	5	sec	5	5	5	5	5	5
12.	Screw speed	200	rpm	200	200	200	200	200	200
13.	Back pressure	1	bar	1	1	1	1	1	1
14.	Cooling time	20	sec	20	20	20	20	20	20
15.	Cycle time	-	sec	38	38	40	38	40	40

The injection molding parameters applied for the set and actual production of CNF-filled GF/PPS hybrid nanocomposite specimens (C0–C5) are summarized in Table 6. The statistics suggest that the processing conditions were almost comparable for all formulations with just small differences in cycle time, barrel temperature and injection pressure. Such a controlled procedure is necessary to reduce the manufacturing variability and to ensure that the differences in the measured attributes are mostly attributable to the change in the CNF concentration and not to the conditions of the molding process. Therefore, the uniform injection molding settings allow a reliable comparison of all composite samples and ensure a reproducibility of the manufacturing process.

The raw material compositions used to produce PPS-based hybrid nanocomposites with different CNF levels ranging from 0 to 1.0 wt% are listed in Table 7. While the PPS content decreased proportionately as the CNF loading increased, the quantity of GFs and stabilizer was maintained at 2000 g and 10 g, respectively. This process of formulation helped standardize the preparation of the materials. The overall weight of all composite samples (C0–C5) in the batch was constant (5000 g).

Table 7. Composition of raw materials of PPS hybrid nanocomposites with 0–1 wt% CNFs.

Composites (Codes)	PPS (g)	SGFs (g)	CNFs (g)	Batch weight (g)	Stabilizer (g)
PPS (C0)	2990	2000	0	5000	10
PPS/CNF 0.2% (C1)	2980	2000	10	5000	10
PPS/CNF 0.4% (C2)	2970	2000	20	5000	10
PPS/CNF 0.6% (C3)	2960	2000	30	5000	10
PPS/CNF 0.8% (C4)	2950	2000	40	5000	10
PPS/CNF 1.0% (C5)	2940	2000	50	5000	10

2.3 Characterization

2.3.1 Scanning electron microscopy

Field emission scanning electron microscopy (ZEISS SIGMA FESEM) was used to analyse the microstructure and worn surfaces of the composites to identify damage and wear mechanisms and correlate them with experimental results. To enhance image quality, selected specimens were coated with a thin gold layer prior to observation. Images were acquired using both secondary and backscattered electron modes, enabling assessment of surface features as well as particle size and distribution associated with the wear processes.

2.3.2 Density measurement and voids

A METTLER AE 200 densitometer, which is based on the Archimedes principle, was used to measure the density of the manufactured composites in compliance with ASTM D792-08 [36]. For testing, specimens measuring 25 mm by 10 mm by 3.2 mm were cut from 100 mm molded composite disks. The average density was given after 2 measurements were made for each composite series to ensure accuracy and repeatability. Using Eqs. (1) and (2), the theoretical composite density (ρ_{ct}) and the empirically determined density were compared to get the void content (V_v).

$$\rho_{ct} = \frac{1}{(W_f/\rho_f)+(W_m/\rho_m)+(W_{pf}/\rho_{pf})} \quad (1)$$

where, W_f, W_m and W_{pf} are wt% of fiber, matrix and particulate filler respectively. ρ_f, ρ_m and ρ_{pf} are density of fiber, matrix and particulate filler respectively.

$$V_v = \frac{\rho_{ct} - \rho_{ce}}{\rho_{ct}} \quad (2)$$

where, ρ_{ct} and ρ_{ce} are theoretical density and experimental density of the composite samples.

2.3.3 Interlaminar shear strength test

The short-beam shear test was used to measure the interlaminar shear strength (ILSS) of the produced PPS-based hybrid nanocomposites in compliance with ASTM D2344M-22 [37]. The span-to-depth ratio of the prepared specimens was 6:1 (specimen width = 2 × thickness). A universal testing machine

(UTM-Kalpak Instruments & Controls, Pune, India) with a three-point bending configuration was used to conduct the test. Up until failure, the specimen was centrally loaded at a steady crosshead speed of 1 mm/min. The necessary span-to-thickness ratio was maintained by carefully adjusting the support span. Three duplicate specimens were evaluated at 23 °C and a crosshead speed of 1 mm/min for each formulation. The findings are displayed as mean ± standard deviation, and coefficients of variation less than 3.9% indicate exceptional repeatability. The standard relation was used to compute the ILSS:

$$ILSS\ (MPa) = \frac{0.75 \times P_{max}}{B \times H} \quad (3)$$

Where, P_{max} refer to maximum load at failure in N, B stands for width in mm, and H refers to specimen thickness in mm.

2.3.4 Hardness measurement

For all composite series, the samples were sectioned according to standard dimensions. PPS-based hybrid nanocomposites' Barcol hardness was assessed using ASTM D2583-13a [38]. Using an indenter positioned perpendicular to the specimen surface, ten indentations were made per sample, spaced to prevent interference. Following stabilization, measurements were taken and the mean values ± standard deviation were computed from ten replicate specimens per composition for analysis.

2.3.5 Three-body abrasive wear test

In compliance with ASTM G65, three-body abrasive wear (3BAW) tests were carried out utilizing a dry sand/rubber wheel abrasion tester (Magnum Engineers, Bangalore, India) [39]. Photograph containing specifics of the test setup are displayed in Figure 5. A chlorobutyl rubber wheel (58–62 Shore A) spinning at 200 rpm was placed between the specimen and angular silica sand, which was employed as the abrasive at a feed rate of 255 ± 5 g/min. Abrasives utilized in this study were silica sand (ρ = 2600 kg/m^3; Knoop hardness 880). In the present study, silica sand (ρ = 2600kg/m^3; Knoop hardness 880 was used as abrasives. Figure 6 (a) and (b) show the photography and SEM images of dry silica sand particles at 100× magnification with a 100 μm scale bar, which are appropriate for assessing abrasives in 3BAW tests where loose particles remove material through cutting, ploughing, and rolling actions.

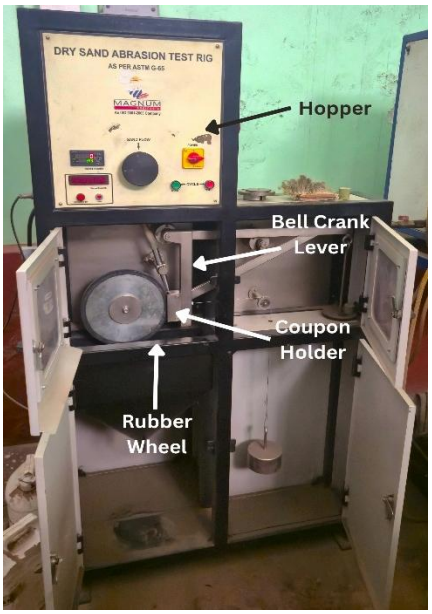

Fig. 5. Photograph of the dry sand rubber wheel abrasion tester.

(a)

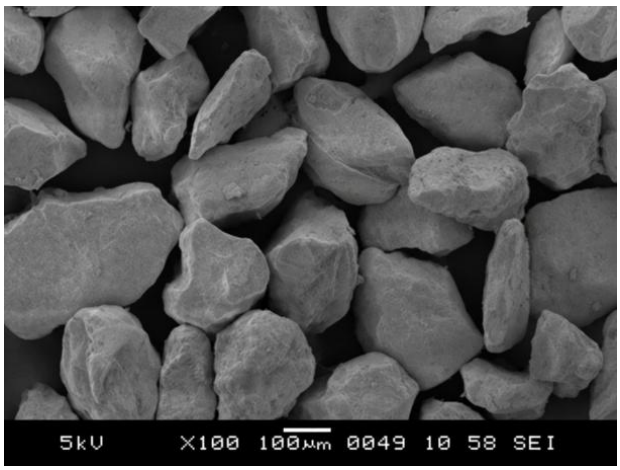

(b)

Figure 6. (a) Photographic image of silica sand particles (200–300 μm), (b) Photomicrograph of silica sand particles.

The average equivalent diameter of the sand particles, derived from many grains of 1.5–2.5 scale bar lengths, is roughly 200–300 μm. In ASTM G65 3BAW tests, medium-grade abrasives (such as 50–70 mesh sand) are utilized, and particles in this size range facilitate efficient wear without causing undue fragmentation at first. In the SEM image, the fragmented surfaces and projecting asperities show irregular, angular to sub-angular shapes with jagged edges and low sphericity. Because of its medium size and angular shape, the sand is perfect for use as a dry abrasive in 3BAW tests. This allows for uniform micro cutting on specimens that are being loaded against a revolving wheel.

Table 8. Factor and levels for 3BAW tests

Factor	Designation	Level		
		I	II	III
Filler content (wt %)	A	0	0.4	0.8
Abrading Distance (m)	B	250	500	750
Applied Load (N)	C	5	10	15

The 3BAW tests were designed by using the BBD which is a regularly used DoE method under RSM. This method is notably suitable for the development of quadratic response models with reduction of experimental trials in comparison with the full-factorial or central composite designs. This reduces the time, material consumption and experimental cost while prediction accuracy is maintained. When harsh testing conditions are neither desirable nor unfeasible, its elimination of corner-point combinations also makes it preferable [40-42]. Minitab Statistical Software (Version 22.1, PA, USA) was used to build the experimental matrix. The selected control factors and their levels are shown in Table 8. Previous to each test, specimens were oven dried, ultrasonic cleaned in acetone, and weighed with a balance of 0.0001 g precision. The standard load was kept constant throughout the experiment in the abrasion test. Upon completion of the test, the specimens were cleaned, dried and reweighed to determine the material loss due to wear.

3. RESULTS AND DISCUSSION

3.1 Microstructure of PPS-based hybrid nanocomposites

To comprehend the dispersion of CNFs, fiber–matrix interfacial properties, and fracture mechanisms controlling the overall performance of the produced composites, microstructural analysis was performed. Direct proof of load transfer efficiency, crack propagation behavior, and the function of CNFs in network creation inside the PPS matrix can be obtained by examining the cracked surfaces.

Figure 7(a, b) shows the cryo-fractured morphology of the GF/PPS composite without CNFs (sample C0). Several smooth fiber pull-out cavities, exposed fiber ends, broken fibers, and obvious interfacial gaps between the GF and PPS matrix are apparent in the SEM pictures. Additionally, distinct river marks and matrix fracture regions are seen, suggesting the propagation of brittle cracks into the matrix. Inadequate fiber–matrix adhesion, which restricts efficient stress transfer from the PPS matrix to the reinforcing fibers, is confirmed by the preponderance of clean fiber surfaces and debonded interfaces. Interfacial failure is the primary fracture mechanism, as indicated by the comparatively large percentage of pull-out features and void spaces found in qualitative image assessment.

On the other hand, the fracture morphology of the hybrid nanocomposite with 0.8 wt% CNFs (sample C4) in Fig. 7(c, d) is noticeably different. While fragmented fibers stay more firmly lodged inside the matrix, exhibiting greater interfacial anchoring, the number of fiber pull-out cavities is greatly decreased. Higher energy absorption during crack propagation is suggested by the cracked PPS surface becoming rougher and more winding. Additionally, increased CNF dispersion and the development of a semi-continuous reinforcing network inside the PPS matrix are indicated by evenly dispersed nanoscale fibrillar characteristics around the fibers. This network improves load transmission efficiency by bridging microvoids and limiting fracture formation.

Thus, CNF incorporation significantly increases dispersion uniformity, decreases interfacial debonding flaws, and encourages cohesive fracture behavior, according to a qualitative picture comparison between Figs. 7(a, b) and 7(c, d). The synergistic impact of CNFs, which increase matrix stiffness, improve mechanical interlocking at the GF/PPS interface, and produce conductive nanoscale channels that resist

fracture initiation and propagation, is responsible for the enhanced bonding seen in sample C4. The observed improvement in the mechanical and tribological performance of the produced hybrid nanocomposites is substantially supported by these microstructural changes.

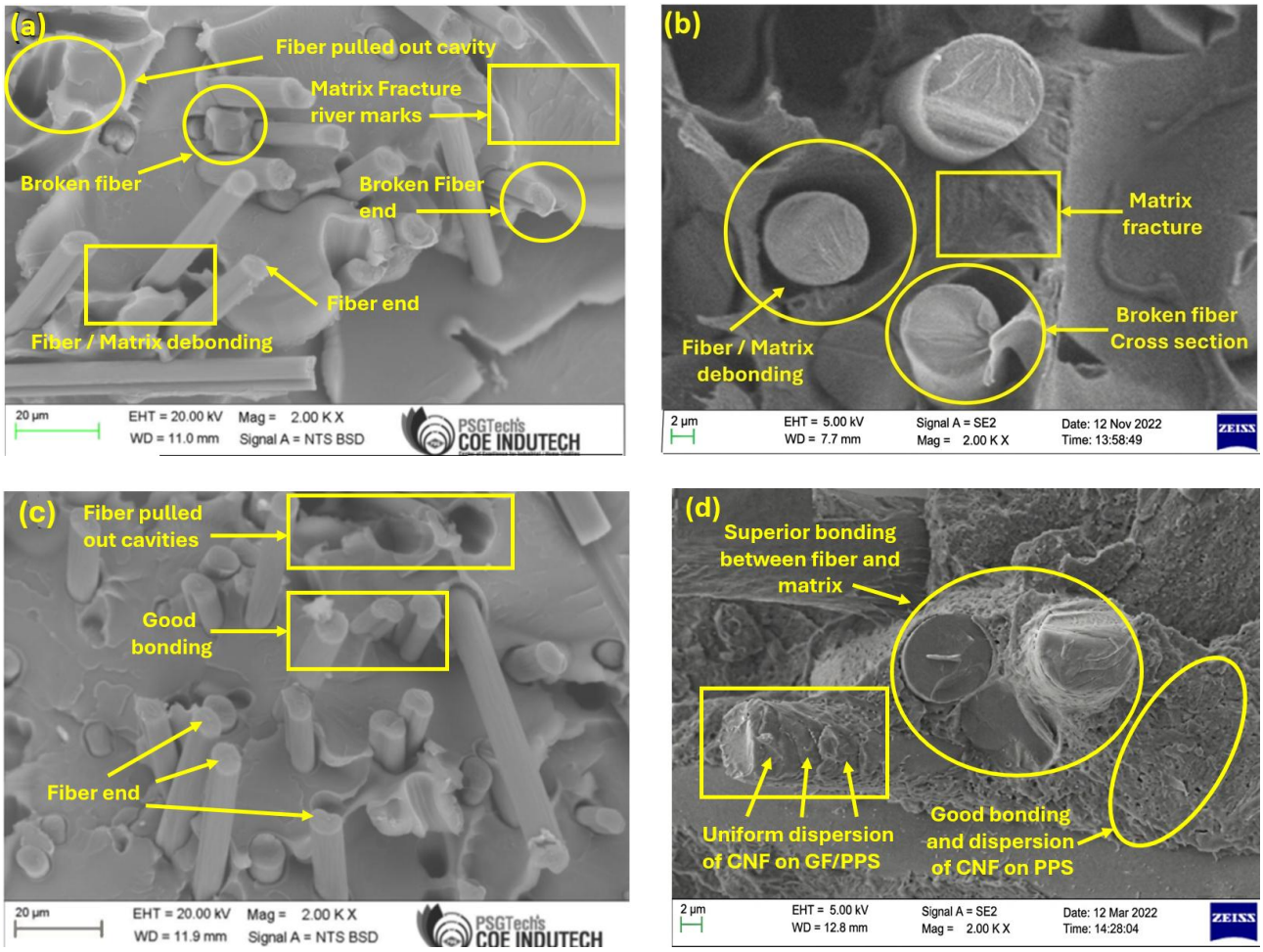

Fig. 7. Microstructure of cryo-fractured PPS-based composites: (a, b) GF/PPS (C0). (c, d) CNF filled GF/PPS (C4) hybrid composites.

3.2 Density and void content analysis of PPS-based hybrid nanocomposites

The mechanical performance, durability, and structural integrity of fiber-reinforced thermoplastic composites are significantly influenced by the density and void percentage of the material. The void content created during composite manufacturing was estimated in the current work by comparing the theoretical and experimental densities of CNF filled GF/PPS hybrid composites. The density and percentage of voids for composites C0–C5 as their CNF content increases are summarized in Table 9. The rule of mixtures, which connects a composite's density to the density and wt% of its constituents, was used to evaluate the theoretical density of the composites.

The amount of void content in the manufactured composite can be estimated from the difference between theoretical and experimental density.

The baseline composite GF/PPS (C0, Table 9) has an extremely low void content of 0.31% with a theoretical density of 1.624 g/cm^3 and an experimental density of 1.619 g/cm^3. This suggests good fiber wetting and efficient consolidation throughout processing. The void content increased to 0.67% when a little amount of CNF (0.2 wt%) was added to composite C1. The theoretical density marginally increased to 1.631 g/cm^3 but the experimental density remained relatively lower at 1.62 g/cm^3. The tendency of nanofibers to agglomerate, which might impede appropriate resin flow and lower the packing efficiency inside the composite structure, may be the cause of the rise in void fraction with low CNF

loading [43]. With an experimental density of 1.625 g/cm^3 and a theoretical density of 1.638 g/cm^3 when the CNF concentration rose to 0.4 wt% (C2), the void fraction was 0.79%. The increase in voids % indicates that as nanofiller loading increases, dispersion issues become more important.

Table 9. Density and voids of fabricated CNF filled GF/PPS hybrid nanocomposites.

Composites (Codes)	Density (ρ_t g/cm^3)	Density (ρ_e g/cm^3)	% Voids	Hardness (Barcol)	% increase	ILSS (MPa)	% increase
C0	1.624	1.619 ± 0.2	0.31	44.2 ± 0.3	---	28.7 ±1.3	---
C1	1.631	1.620 ± 0.3	0.67	47.2 ± 0.2	6.79	29.9 ±1.2	4.18
C2	1.638	1.625 ± 0.2	0.79	48.9 ± 0.2	10.63	31.3 ±1.1	9.06
C3	1.642	1.631 ± 0.1	0.67	51.8 ± 0.3	17.19	33.1 ±1.3	15.33
C4	1.667	1.659 ± 0.2	0.48	54.3 ± 0.2	22.85	35.5 ±1.2	23.69
C5	1.654	1.635 ± 0.4	1.15	50.8 ± 0.4	14.93	30.9 ±1.5	7.67

Supplier's data: Density of E-GF 2.54 g/cm^3, Density of CNF 2.1 g/cm^3, Density of PPS 1.35 g/cm^3

Due to their large surface area and potent van der Waals interactions, nanofibers can cause localized resin starving areas during processing and encourage agglomeration [44]. It's interesting to note that the GF/PPS dropped to 0.67% at 0.6 wt% CNF. This decrease could be a sign of better filler dispersion and increased interfacial interaction between the nanofillers, SGF reinforcement, and PPS matrix. When evenly distributed throughout the polymer matrix, CNFs can serve as secondary reinforcement, enhancing packing density and filling micro-voids [45].

Composite C4 with 0.8 wt% CNF showed a more pronounced improvement. With theoretical and experimental densities of 1.667 and 1.659 g/cm^3, respectively, the void fraction was comparatively low at 0.48%. By occupying interstitial areas within the composite structure, an ideal CNF loading may increase fiber/matrix interfacial bonding and decrease micro-porosity, according to the improved densification. Similar findings have been documented in hybrid fiber nanocomposites, where void formation is decreased and packing efficiency is increased by nanoscale fillers [46]. Despite the theoretical density being reasonably high (1.654 g/cm^3), the void fraction dramatically increased to 1.15% when the CNF content increased to 1.0 wt% (C5). This increase can be explained by the PPS matrix's increased melt viscosity and agglomeration caused by an excessive nanofiller content. Increased viscosity causes void formation by limiting resin flow during composite manufacturing and encouraging air pocket entrapment [47]. Overall, the obtained results show that the density and void formation behavior of GF/PPS composites are affected by the addition of CNF. While excessive loading causes agglomeration and increased porosity, moderate CNF loading (around 0.6–0.8 wt%) seems to encourage improved packing and less void formation. Since voids serve as stress concentration sites that seriously impair mechanical qualities like strength, fatigue resistance, and interlaminar shear performance, maintaining a low void content is crucial [48].

3.3 Hardness of PPS-based hybrid nanocomposites

Polymer composites' surface hardness offers important information on the material's stiffness, interfacial adhesion, and resistance to localized deformation. This study evaluated the Barcol hardness of GF/PPS composites reinforced with different content of CNF in accordance with ASTM D2583. The results show that CNF addition greatly influences the surface mechanical performance of the hybrid composites, as shown in Table 9.

A moderate hardness of 44.2 ± 0.3 was shown by the baseline composite (C0), which was composed of PPS reinforced with 40 wt% GFs. The addition of SGF further increases the matrix's ability to support loads through better load distribution. PPS is a semicrystalline thermoplastic that is well-known for its excellent rigidity and thermal stability [49]. The Barcol hardness improved by 6.79% and 10.63%, respectively, to 47.2 (C1) and 48.9 (C2) after tiny amounts of CNF (0.2–0.4 wt%) were added. The high modulus and nanoscale reinforcing impact of CNFs are responsible for

this improvement. CNFs strengthen resistance to indentation and restrict the mobility of PPS polymer chains because of their high aspect ratio and mechanical hardness. Additionally, load transmission between the matrix and reinforcing fibers is enhanced by these fillers [46]. Interestingly, the inherent stiffness of the nanofibers more than made up for these microstructural defects even though the void content increased marginally in these early stages (0.67–0.79%).

At CNF concentrations of 0.6–0.8 wt%, the hybrid reinforcing effect became most noticeable. The Barcol hardness increased by 22.85% over the baseline, reaching 51.8 (C3) and summiting at 54.3 (C4). At these concentrations, the CNFs serve as additional reinforcement that improves interfacial bonding and load transmission efficiency by successfully bridging the interface between the GFs and the PPS matrix. The successful reinforcement of the fiber–matrix interface by CNF nanoparticles is confirmed by the simultaneous increase in ILSS and hardness [47]. A denser structure and better mechanical integrity may result from increased packing efficiency, as indicated by the decrease in microvoids at these levels [47].

Nevertheless, the Barcol hardness changed to 50.8 ± 0.4 when CNF loading was raised to 1.0 wt% (C5). High van der Waals forces that produce nanofiber aggregation are primarily responsible for this reduction. These agglomerates restrict the effective reinforcing capacity of the nanofibers and produce localized stress concentration zones [48]. High nanofiller loading also makes the PPS melt more viscous during processing, which might obstruct resin flow and trap air. The density investigation in Table 9, which reveals that C5 has the highest void content (1.15%), supports this. In the end, these microstructural flaws reduce the composite's overall surface integrity and restrict hardness improvement.

3.3 Interlaminar shear strength of PPS-based hybrid nanocomposites

The short-beam shear test was used to assess the interlaminar shear strength (ILSS) of the GF/PPS/CNF composites in accordance with ASTM D2344/D2344M (ASTM International, 2022). The interfacial bonding between the polymer matrix and reinforcement, which establishes the composite's resistance to delamination under shear stress, is indicated by ILSS.

With the addition of CNF, the ILSS of CNF-filled GF/PPS hybrid nanocomposites rose, suggesting better bonding between the PPS matrix and GFs (Table 9). The ILSS of the control composite (C0) was 28.7 MPa. Well-dispersed CNFs improve stress transmission and resistance to interlaminar failure, as demonstrated by the ILSS improvements of 4.18%, 9.06%, and 15.33% for Composites C1, C2, and C3, respectively. CNFs' high aspect ratio and nanoscale size encourage mechanical interlocking and strengthen the polymer matrix [49]. Of all the samples, C4 had the highest ILSS of 35.5 MPa, which was 23.69% higher than C0. Uniform CNF dispersion, efficient load transfer, and crack-bridging mechanisms inside the PPS matrix are responsible for this improvement. Similar improvements in interlaminar strength brought about by CNF insertion have also been documented in fiber-reinforced polymer composites, where nanofibers boost interfacial adhesion and delamination resistance [50].

Even with the lower ILSS value of 30.9 MPa, C5 outperformed the baseline composite by 7.67%. Higher void content (1.15%) and CNF agglomeration, which produce stress concentration sites and lessen effective stress transfer, may be the cause of the decrease. Reduced mechanical performance and dispersion problems might result from excessive CNF loading [51]. Because of its enhanced interfacial bonding and effective stress transfer, C4 was shown to be the ideal CNF loading for optimizing ILSS.

3.4 Modeling and optimization of wear loss of PPS-based hybrid nanocomposites

3.4.1 Design of experiments

Using Minitab® 21 software, RSM based on Box–Behnken Design (BBD) was used to assess the 3BAW loss of hybrid nanocomposites under various operating situations. BBD was chosen because it is a cost-effective and efficient approach for creating second-order prediction models that capture the main effects, quadratic terms, and interactions between variables with fewer experimental trials. A full factorial design would need 27 runs for three variables at three levels,

while BBD only needed 15 runs (12 edge points + 3 center points), saving money, time, and material.

Over 60% of the experimental runs were repeated in order to increase the dependability of the data, and the average values were analyzed. Consistent test protocols and instrument calibration reduced measurement uncertainty. But it's important to recognize that BBD has some limits. The design may not be able to capture extremely nonlinear behavior close to border regions since it does not incorporate all combinations at extreme factor levels. Furthermore, the very modest number of runs might limit more extensive applicability beyond the studied region. However, within the chosen process window, the created model demonstrated adequate predictive capability. The resilience and prediction accuracy of the model may be further improved by future research employing more datasets and broader design spaces.

According to Table 6, the input variables were applied load (N: 5, 10, 15), abrading distance (m: 250, 500, 750), and nanofiller loading (wt%: low (0), medium (0.4), high (0.8)). The DoE module in Minitab® 21 was used to randomly build the 15-run BBD matrix (Table 10), ensuring orthogonal blocking and rotatability for dependable quadratic response modeling.

Table 10. Experimental design for wear loss analysis of PPS-based hybrid nanocomposites.

Filler wt%	Abrading Distance (m)	Applied Load (N)	Wear loss (g)
0	750	10	0.5189
0.4	500	10	0.4101
0.8	750	10	0.2290
0	250	10	0.5112
0.4	250	5	0.1248
0.4	750	15	0.4589
0.8	500	5	0.1448
0.4	250	15	0.4948
0.4	500	10	0.4101
0.8	250	10	0.2180
0.8	500	15	0.2389
0	500	15	0.4575
0.4	500	10	0.3201
0	500	5	0.3260
0.4	750	5	0.1997

3.4.2 Analysis of variance

As per Table 10, GF/PPS/CNF hybrid nanocomposite samples from the 3BAW experiments are displayed in Figure 8. Figure 8(b) shows post-abrasion samples with discernible black wear tracks, surface roughening, and material loss on the pink matrix, while Figure 8(a) shows pristine samples with uniform, smooth cyan-colored surfaces before abrasion. The pictures show common wear damage mechanisms, such as particle dissociation and micro-ploughing under BBD conditions. These visible alterations validate measurable wear loss as the study's main response variable.

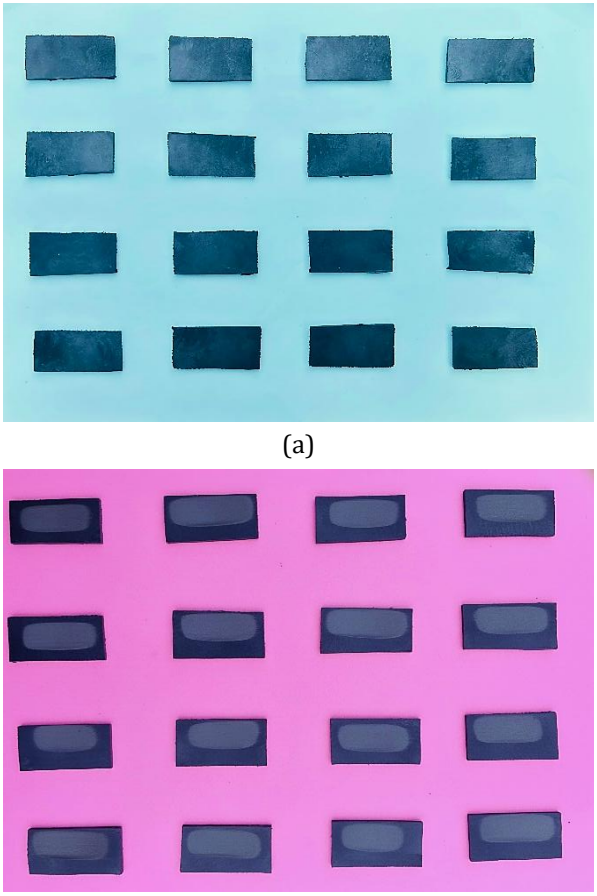

(a)

(b)

Fig. 8. 3BAW test samples: (a) Before wear test, (b) After wear test.

Table 11 summarizes the findings of an analysis of variance (ANOVA) that was used to determine the important process variables influencing wear loss of PPS-based hybrid nanocomposites. With an overall F-value of 5.05 and a P-value of 0.045 (<0.05), the constructed quadratic regression model was determined to be statistically significant, indicating that it accurately describes the

experimental data. With R^2 = 86.87% and adjusted R^2 = 83.29%, the model demonstrated good predictive performance, suggesting that model terms account for the majority of the variation in wear loss. This updated modified R^2 score addresses the previous issue of poor predictive adequacy and shows a good model fit.

The linear terms were the main causes of wear loss among the factors under investigation. The most significant factor was filler weight percentage (F = 22.96, P = 0.005), followed by applied load (F = 17.37, P = 0.009), indicating that load and CNF content had a significant impact on tribological behavior.

Table 11. ANOVA results for wear loss of PPS-based hybrid nanocomposites.

Source	DF	Adj SS	Adj MS	F-Value	P-Value
Model	9	0.238871	0.026541	5.05	0.045
Linear	3	0.212470	0.070823	13.47	0.008
Filler wt%	1	0.120712	0.120712	22.96	0.005
Abrading Dist (m)	1	0.000422	0.000422	0.08	0.788
Applied load (N)	1	0.091335	0.091335	17.37	0.009
Square	3	0.022994	0.007665	1.46	0.332
Filler wt%*Filler wt%	1	0.002497	0.002497	0.47	0.521
Abrading Dist (m)*Abrading Dist(m)	1	0.000012	0.000012	0.00	0.964
Applied load (N)*load (N)	1	0.021175	0.021175	4.03	0.101
2-Way Interaction	3	0.003407	0.001136	0.22	0.881
Filler wt%*Abrading Distance (m)	1	0.000003	0.000003	0.00	0.982
Filler wt%*Load (N)	1	0.000346	0.000346	0.07	0.808
Abrading Dist (m)*Load (N)	1	0.003058	0.003058	0.58	0.480
Error	5	0.026287	0.005257		
Lack-of-Fit	3	0.024620	0.008207	9.85	0.094
Pure Error	2	0.001667	0.000833		
Total	14	0.265158			

R^2 (86.87%), R^2 adj (83.29%)

Abrading distance, on the other hand, exhibited no statistically significant impact (P = 0.788). Wear loss within the chosen design range was primarily governed by linear factor responses rather than higher-order interactions, as indicated by the statistical insignificance of the quadratic terms and two-way interaction effects (P > 0.05). The regression coefficients' confidence intervals were also looked at, and they matched the significance trends seen in the ANOVA table.

The appropriateness of the chosen BBD model is further validated by the lack-of-fit P-value of 0.094 (>0.05), which shows that the model error is not substantial in comparison to pure experimental error. Over 60% of the runs were repeated, and average values were used to improve reliability. Furthermore, the model prediction error stayed around 5%, suggesting that the predicted and experimental responses agreed well.

The residual points nearly follow the reference straight line in the normal probability plot of residuals (Fig. 9), indicating the approximate normal distribution of errors and the lack of significant outliers. This demonstrates that the generated regression model can be utilized to accurately forecast wear loss within the examined parameter range and confirms the ANOVA's underlying assumptions.

3.4.3 Regression model development and validation

The wear loss of PPS-based hybrid nanocomposites under 3BAW conditions was quantitatively correlated with process factors using Response Surface Methodology (RSM). A second-order polynomial regression model was created to forecast wear loss as a function of filler content, abrading distance, and applied force based on the

Box–Behnken experimental design. The whole coding regression formula is written as follows:

$$Y=0.39343-0.12284A+0.00726B+0.10685C+0.00088AB-0.00930AC-0.02765BC-0.02600A^2+0.00180B^2-0.07573C^2 \quad (4)$$

A = Filler wt%; B = Distance; C = Load

The regression coefficients show how each element affects wear loss in relation to the others. Because of increased hardness, load-bearing capacity, and resistance to abrasive penetration, a higher CNF content minimizes wear loss, as confirmed by the negative linear coefficient of A (-0.12284). Conversely, the positive coefficients of B (0.00726) and C (0.10685) show that wear loss increases with increasing abrading distance and applied load. Higher load increases contact pressure, which encourages micro-cutting and ploughing, while longer abrading distance promotes cumulative surface damage. Among the interaction factors, the modest positive AB term suggests a minor combined contribution of filler content and distance, while the negative coefficients of AC and BC suggest that filler addition partially compensates the negative effect of load and distance. Curvature effects and the existence of ideal filler loading and applied load levels within the examined range are shown by the negative quadratic coefficients of A^2 and C^2. When it comes to predicting wear loss and optimizing processing parameters, the regression model provides a reliable approach. To evaluate the appropriateness and predictive potential of the built regression model, confirmation tests were conducted using particular parameter combinations that were not directly used in the model fitting. The experimental setup for the confirmation testing is displayed in Table 12.

Table 12. Confirmation test parameters for wear loss.

Trials	Filler wt%	Abrading Distance (m)	Applied Load (N)
1	0	600	12
2	0.4	600	12
3	0.8	600	12

A rubber wheel abrasion tester was used for the confirmation trials, and the wear loss values acquired from the experiment were compared to the regression model's predictions. Table 13 summarizes the findings of this comparison.

Table 13. Confirmation test data for wear loss of hybrid nanocomposites.

Trials	Experimental Wear Loss (g)	Predicted Wear Loss (g)	% Error
1	0.5759	0.5451	5.35
2	0.4372	0.4105	5.02
3	0.2894	0.2759	4.66

Confirmation experiments were used to verify the created RSM model's reliability; the results are shown in Table 13. For every validation trial, there was a strong correlation between the experimental and expected wear loss values. The percentage error was within acceptable bounds for tribological experiments using polymer composites, ranging from 4.66% to 5.35%. This minimal variation demonstrates that the regression model correctly accounts for the effects of applied load, abrading distance, and CNF content on wear loss. As a result, within the examined design range, the proposed model may be regarded as dependable for both parameter optimization and wear behavior prediction.

Furthermore, the reinforcing effect of CNFs, which improve resistance to abrasive indentation and micro-fracture, is confirmed by the decrease in wear loss with increasing filler content during the confirmation tests. The developed regression equation can accurately estimate wear loss within the examined parameter range, as demonstrated by the tight connection between experimental and anticipated findings. This makes it valuable for material design and process optimization.

Overall, the validation results show that by optimizing filler loading and operating circumstances, the RSM-based model offers a reliable statistical tool for forecasting three-body abrasive wear behavior and enhancing the durability of GF/PPS hybrid nanocomposites.

The current study's findings that wear loss decreases as filler content increases are in line with earlier research on FRPCs using nanofillers. Influence of MoS_2 nano filler additions on wear behavior of CF/epoxy composites, for instance, found that adding MoS_2 nanoparticles greatly increased the 3BAW resistance of CF- composites, resulting in a nearly 35% decrease in wear under high abrading distance because of better load transfer and the creation of a protective tribo-film on the sliding surface [17]. In a similar vein,

increasing the amount of microcrystalline cellulose (MCC) in epoxy-based composites reinforced with natural fibers has been found to improve resistance to abrasive wear. An ideal MCC loading (6 wt%) shows the lowest three-body abrasive wear because of improved load transfer, crack deflection, and the creation of a protective tribolayer [52]. The addition of MCC improves interfacial bonding and surface hardness, resulting in improved mechanical strength and tribological performance.

This trend is further supported by recent research on hybrid fiber composites. The addition of MCC fillers enhanced interfacial bonding and hardness in the hybrid experimental and machine learning approach for optimizing abrasive wear of MCC modified hemp/bamboo fiber composites, leading to lower 3BAW and milder wear mechanisms when compared to baseline composites [53]. Together, these results corroborate the current findings, which show that fiber reinforcing and nanofiller insertion improve hardness, load-bearing capacity, and matrix–fiber interface strength, consequently decreasing material removal during three-body abrasion. The reliability of the established full regression model for forecasting wear behavior in fiber-reinforced thermoplastic nanocomposites is further supported by the concordance between the current results and earlier research.

A normal probability plot of residuals, where points roughly following a straight line indicate normality of the residuals, can be used to evaluate the residual errors' normality, which is one of the essential assumptions of ANOVA and regression analysis [54]. Verifying normality is crucial since it ensures the reliability of significance tests for the input parameters and the statistical correctness of the created RSM model.

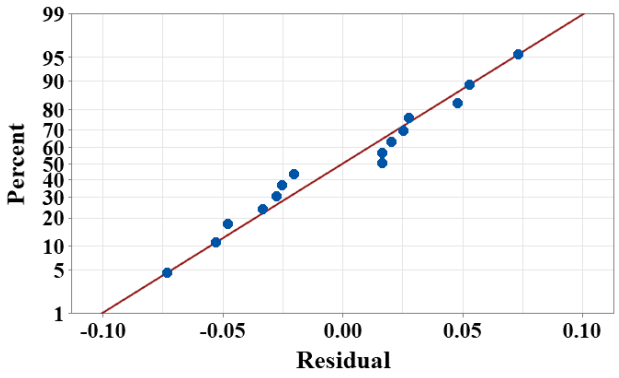

Fig. 9. Normal probability plot for residuals for wear loss.

The majority of residual data points, as illustrated in Fig. 9, are near the straight reference line with just slight deviations at extreme. This pattern suggests that the residuals have a roughly normal distribution and that the dataset is free of significant skewness, aberrant fluctuation, or significant outliers. Additionally, the residuals' symmetric and random distribution implies that the model errors are stable and independent throughout the experimental range. As a result, the normal probability plot verifies that the regression model that was constructed is statistically sufficient and can be utilized with confidence to forecast wear loss of the hybrid nanocomposites under the examined process circumstances.

By analyzing the assumptions of independence, constant variance, and model suitability, residual diagnostic plots were utilized to further confirm the acceptability of the proposed regression model. These charts assist in determining whether the forecast errors are random/model still fails to account for any hidden systemic trends.

The residuals vs observation order plot is shown in Figure 10(a). Throughout all 15 experimental runs, there is no discernible cyclic tendency, drift, or clustering in the residuals, which are dispersed randomly around the zero-reference line. This random distribution shows that the residuals are independent and that the experimental outcomes were unaffected by time-related or sequence-based effects. Therefore, bias was not introduced into the wear loss data by the order of experimentation.

The residuals against fitted values plot, which is frequently used to evaluate homoscedasticity and the suitability of the regression model, is displayed in Figure 10(b). The residuals show almost constant variance over the anticipated wear loss range since they are dispersed on both sides of zero without any discernible curve or funnel-shaped pattern. Additionally, the lack of systematic structure implies that the chosen quadratic model well captures the connection between wear loss and the input variables. Overall, the diagnostic findings from Fig. 10 verify that the created RSM model is statistically accurate for forecasting wear loss within the examined parameter range and that the regression analysis assumptions are met.

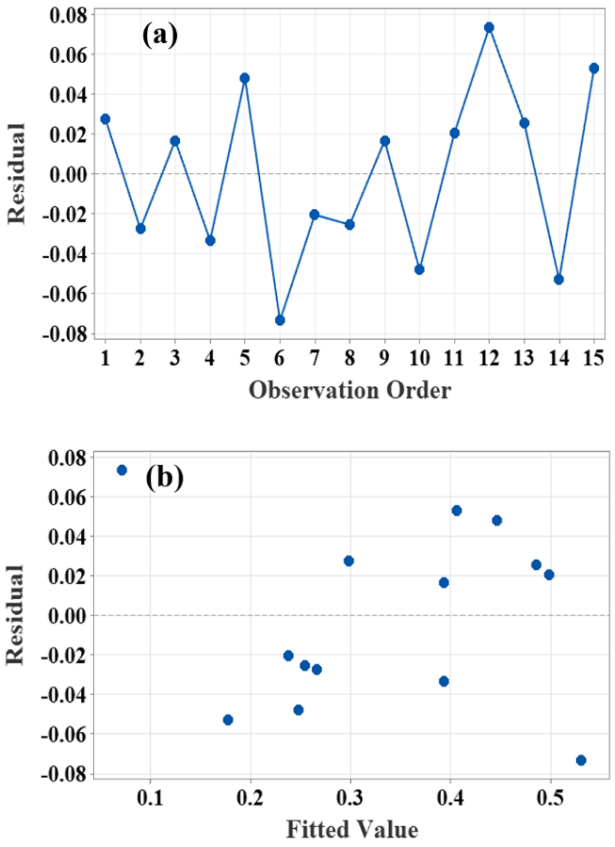

Fig. 10. (a) Residuals vs Observation Order, (b) Residuals vs Fitted Values.

3.4.4 Effect of abrading distance and applied load on wear loss

To illustrate the combined impact of two process parameters on wear loss while maintaining the third factor constant at the center level, contour plots were created. In CNF-filled GF/PPS hybrid nanocomposites, these plots are helpful for determining interaction patterns, optimal parameter zones, and areas linked to the least amount of wear loss.

The relationship between filler wt% and abrading distance is depicted in Figure 11(a). While abrading distance has a relatively minor effect, wear loss significantly decreases as filler content increases. Higher filler loading (around 0.8 wt%) results in the lowest wear region (0.28 g), demonstrating that CNF reinforcement successfully increases abrasion resistance even at longer sliding distances.

The combined effect of applied load and filler wt% is shown in Figure 11(b). Particularly with low CNF content, wear loss dramatically increases with increasing load. Higher filler loading, however, causes the contours to move in the direction of lower wear values, indicating that CNFs improve load-bearing ability and lessen surface damage at higher loads.

The relationship between applied load and abrading distance is shown in Figure 11(c). Wear loss gradually rises from low load/short distance to high load/long distance, demonstrating the combined effect of prolonged abrasive action and higher contact pressure. In a nutshell, the contour plots show that while longer abrading distance and higher applied load encourage material removal, filler weight percentage is the most important element in lowering wear loss.

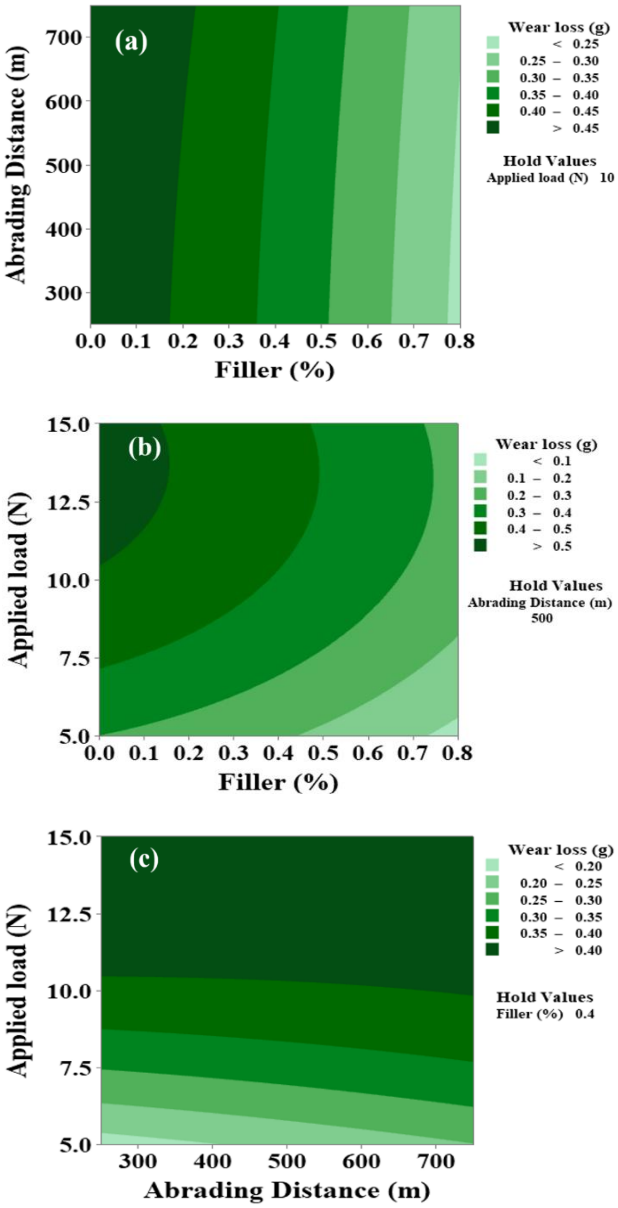

Fig. 11. The contour plot for wear loss: (a) Abrading Distance vs Filler wt%, (b) Applied load vs Filler wt%, (c) Applied load vs Abrading distance.

3.4.5 Main effect plot

By comparing the mean response at various factor levels, the main effects plot was created to assess each process parameter's unique impact on wear loss. The most important variable and the ideal operating range for reducing wear loss in CNF-filled GF/PPS hybrid nanocomposites are shown in Figure 12.

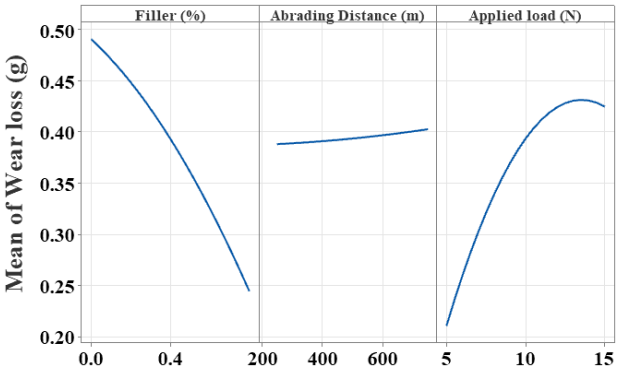

Fig. 12. Main effects plot for wear loss of PPS-based hybrid nanocomposites.

Filler material has the biggest impact on wear behavior, as seen in Figure 12. The typical wear loss significantly drops from roughly 0.49 g to 0.25 g when filler loading rises from 0 to 0.8 wt%. This decrease is explained by CNFs' reinforcing activity, which increases resistance to abrasive wear by improving interfacial bonding, hardness, and load transfer.

Abrading distance has very little effect; wear loss increases slightly between 300 and 700 meters. This suggests that, within the studied range, distance is less important than filler content and applied load.

Wear loss is significantly impacted by applied load. Because of enhanced ploughing action at higher loads, deeper abrasive penetration, and higher contact pressure, the mean wear loss rises from about 0.21 g at 5 N to about 0.43 g at 15 N. Lastly, Figure 12 shows a larger applied load considerably speeds up material removal, filler wt% is the best parameter for minimizing wear loss.

The interaction plot is crucial because it shows how the process parameters namely filler wt%, abrading distance, and applied load are collectively impact the mean wear loss rather than acting individually. It aids in identifying important interactions, in which the degree of one factor influences the effect of another. These insights are crucial for comprehending intricate wear mechanisms, assessing antagonistic or synergistic effects, and figuring out the best combination of parameters to improve the tribological performance of hybrid nanocomposites.

Figure 13 shows how the wear loss of CNF-filled GF/PPS hybrid nanocomposites is affected by the interaction of filler wt%, abrading distance (250, 500, and 750 m), and applied load (5, 10, and 15 N). Increasing the filler content to 0.8 wt% consistently defends against wear, improving structural stability, as seen by the filler (wt%) × abrading distance plot. Conversely, composites with less filler are more vulnerable to material loss, especially when the abrading distance reaches 750 m.

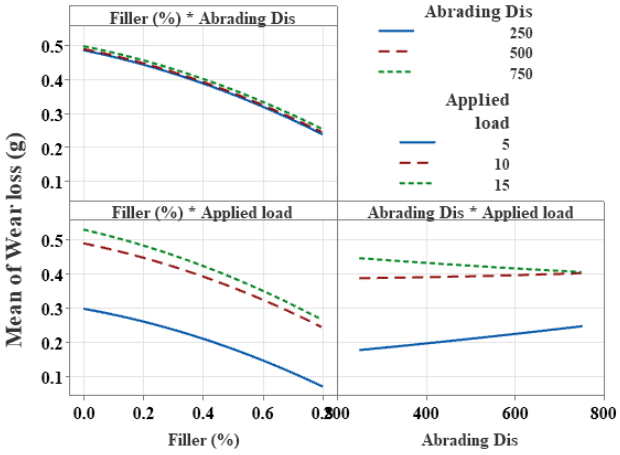

Fig. 13. Interaction plot for wear loss of PPS-based hybrid nanocomposites.

The filler (wt%) × applied load plot further emphasizes the importance of the filler's involvement in load-bearing reinforcement. At lesser loads, the lines stay mostly parallel, but at the highest applied stress of 15 N, there is a noticeable divergence. This suggests that the reinforcing phase becomes crucial at greater stress levels since the wear rates of composites with less filler are much higher than those of their more strongly reinforced equivalents.

Lastly, non-parallel lines that highlight the linked influence of these two parameters are visible in the abrading distance × applied load plot. When longer abrading lengths are combined with higher applied stresses, the overall wear loss increases significantly, indicating a synergistic effect. Such trend implies that optimal filler loading is necessary to reduce severe surface degradation due to the cumulative mechanical stress from both distance and load.

3.4.6 Prediction of wear loss

A multi-response desirability functional analysis was used to optimize the wear performance for CNF-filled GF/PPS hybrid nanocomposites, as shown in the desirability plot (Fig. 14). Finding the exact "sweet spot" where the opposing effects of external mechanical stress and reinforcement concentration cross to result in the least amount of material degradation requires the use of this statistical method. The determined parameters fully satisfy the optimization goal of reducing wear loss within the specified experimental area, as evidenced by the composite desirability value (d) of 1.000.

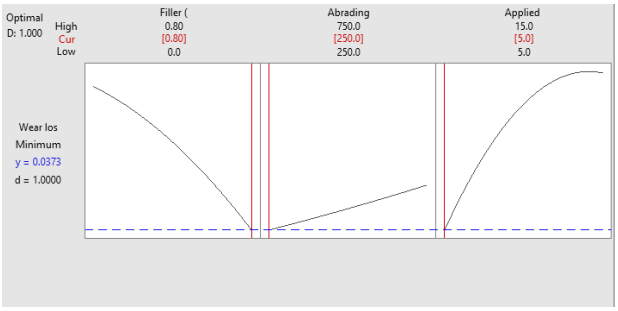

Fig. 14. Desirability plot for wear loss of PPS-based hybrid nanocomposites.

The plot indicates that with a high filler content (0.80 wt%), a short abrading distance (250 m), and a low applied load (5 N), the projected minimum wear loss of y = 0.0373 is reached. The PPS matrix is sensitive to mechanical shearing, as seen by the steep slopes in the load and distance segments of the plot; however, the filler curve's downward trend indicates that the addition of CNF and GFs successfully reduces this damage. The maximum filler content (0.80 wt%) acts as a structural reinforcement to increase the hybrid system's load-bearing capability and move the wear regime closer to the intended minimum.

These findings offer a prediction paradigm for the real-world application of these nanocomposites in high-precision sectors. The model confirms the synergy between the hybrid fillers and the polymer matrix by showing that the lowest wear happens under reinforced, mild-loading situations. The transfer of CNF-filled GF/PPS composites from experimental testing to application-specific design is supported by this prediction accuracy, especially for automotive or aerospace components subjected to light-duty sliding contact where surface lifetime is a crucial need.

3.5 Worn surface morphology

To comprehend the predominant wear mechanisms functioning under 3BAW circumstances, such as micro-cutting, ploughing, particle pull-out, and surface delamination, worn surface morphology in 3BAW is examined. In order to assess the tribological performance of the composites, it also aids in correlating surface damage characteristics with material composition and wear loss.

The effect of CNF content on the wear behavior was evaluated by examining the worn surface morphology of CNF-filled GF/PPS hybrid nanocomposites at an applied load of 15 N and abrading distance of 500 m. The abrasive wear of sample C0 (GF/PPS) was severe with rough wear tracks, deep parallel grooves and debris development, showing the dominant micro-cutting and ploughing of the PPS matrix. Samples C1 (0.4 wt% CNF) and C2 (0.8 wt% CNF) revealed very smooth surfaces with shallow grooves, indicating increased interfacial bonding, load transfer and excellent wear resistance due to CNF reinforcement.

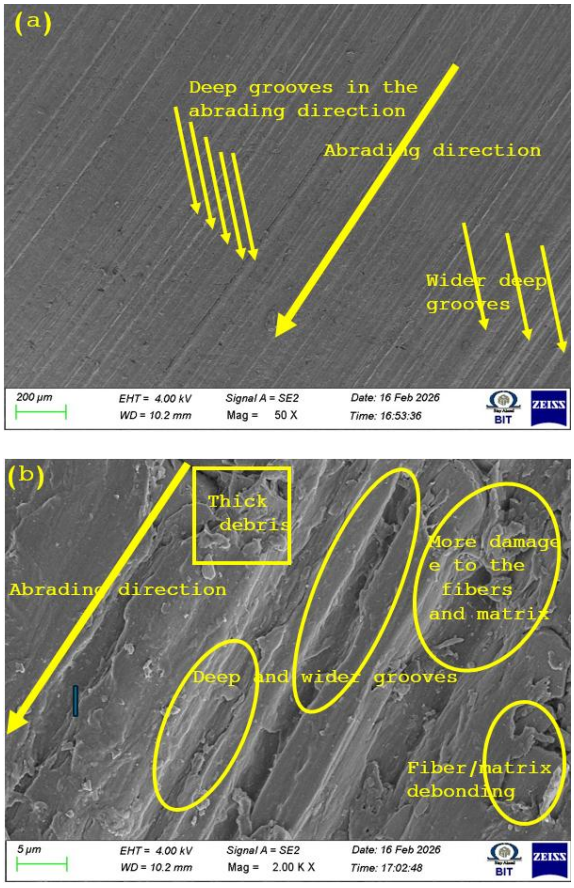

Fig. 15. Worn surface morphology of GF/PPS composite (C0): (a) grooves along abrading direction, (b) deep grooves, debris, and fiber–matrix damage.

The severe micro-ploughing and micro-cutting at higher magnification are shown in Fig. 15b, which confirms that the abrasive wear is intense. The accumulated surface debris functions as third-body abrasive particles to accelerate further the material removal. Also repeated shear forces degrade the fiber-matrix contact, resulting in localized debonding and fiber pull-out. In summary, the worn morphology suggests that micro-ploughing, micro-cutting, interfacial debonding and third-body abrasion are the primary wear mechanisms in sample C0, leading to deep grooves, debris accumulation and substantial wear loss (0.4573 g).

The surface morphology of 0.4 wt% CNF modified hybrid nanocomposite (C1) under load of 15 N and abrading distance of 500 m is depicted in Figures 16a and b. At low magnifications (Fig. 16a) the surface is characterized by thin and narrow grooves in the abrading direction, which can be ascribed to moderate abrasive wear where micro-ploughing is the dominant mechanism. These grooves are considerably less apparent than the ones of the unmodified composite, thus showing less material loss.

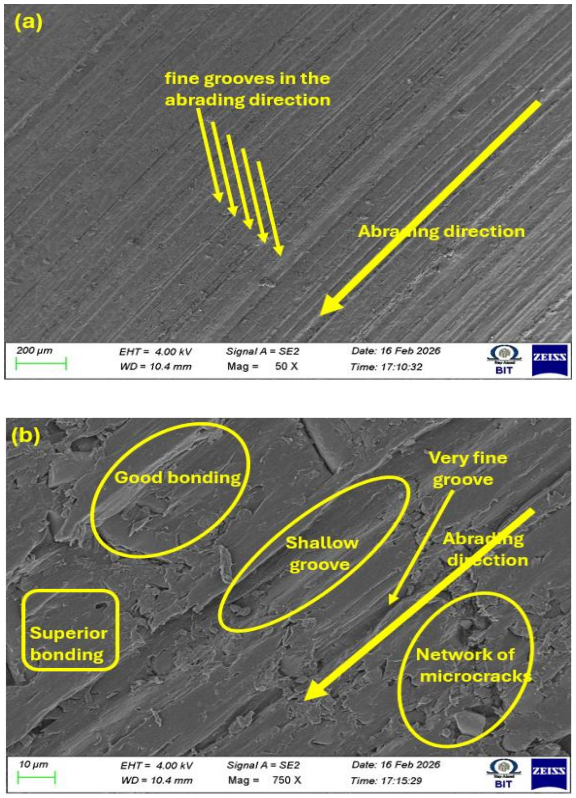

Fig. 16. Worn surface morphology of 0.4 wt% CNF–modified composite (C1): (a) fine grooves along the abrading direction, (b) shallow grooves with improved fiber/matrix bonding.

At higher magnification (Fig. 16b) shallow groove and tiny scratches are indicative of moderate wear. The improved fiber–matrix adhesion with less fiber pull-out evidence that the addition of CNF improves the interfacial bonding between GF and PPS. Repeated shear forces create microscopic microcracks, although their extension appears to be restricted. The surface integrity and wear resistance of C1 composite are generally better than those of C0.

In comparison to the baseline composite (C0), Sample C1's worn morphology (wear loss ≈ 0.4589 g) shows less severe abrasive wear, which is characterized by shallow ploughing, fine grooves, and better fiber–matrix bonding.

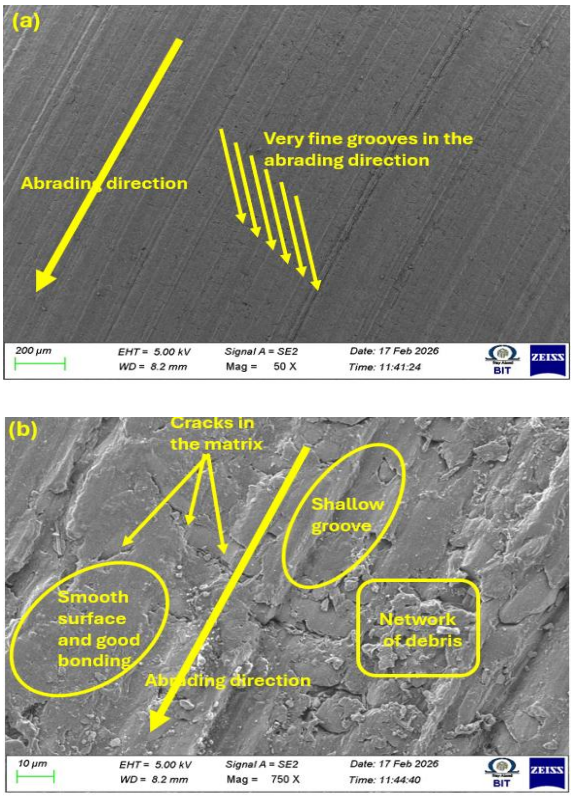

Fig. 17. Worn surface morphology of 0.8 wt% CNF–modified composite (C2): (a) very fine grooves along the abrading direction, (b) smooth surface with shallow grooves, limited matrix cracks, and debris network.

The worn surface morphology of the 0.8 wt% CNF–modified hybrid nanocomposite (C2) tested at a 500 m abrading distance under a 15 N load is depicted in Figures 17a and b. The worn surface shows consistently spaced, extremely thin grooves that line up with the direction of abrading at lower magnification (Fig. 17a). These grooves are shallow and less noticeable, suggesting that mild micro-ploughing with little

abrasive asperity penetration into the PPS matrix dominates the wear mechanism. This implies better surface stability during abrasion and controlled material removal.

The surface becomes relatively smoother with shallow grooves and little scratches at higher magnification (Fig. 17b), indicating a mild abrasive wear mechanism. Additionally, the micrograph demonstrates enhanced fiber-matrix adhesion with little indication of fiber pull-out, suggesting efficient load transfer between the PPS matrix and SGF reinforcement. Furthermore, the worn surface exhibits a small layer of debris that could serve as a protective third-body layer and lessen direct contact between abrasive particles and the composite surface. Overall, Sample C2's worn morphology (wear loss ≈ 0.2389 g) shows improved wear resistance with minor cracking, shallow ploughing, fine grooves, and the production of protective debris.

3.6 Correlation between microstructure, density, hardness and abrasion resistance

The tribological performance of CNF filled GF/PPS hybrid nanocomposites is highly affected by microstructure and mechanical characteristics. interfacial bonding, density, hardness and effective load transfer are contributing factors for the total wear resistance of the composites.

The baseline GF/PPS composite shows the interfacial gaps and poor fiber/matrix adhesion, which act as the stress concentration sites throughout the abrasive wear process. These flaws are conducive to fiber debonding, matrix cracking and fast material removal, leading to increased wear loss. On the other hand, the CNF inclusion develops a conductive reinforcing network around the glass fibers and inside the PPS matrix, enhancing fiber–matrix interaction and limiting crack initiation and propagation under abrasive loading. This microstructural refinement is quantitatively confirmed by the measurements of density and hardness. The moderate addition of CNF (0.6–0.8 wt%) fills the interstitial gaps and boosts the composite densification by boosting the packing efficiency, therefore improving the structural integrity and load bearing capabilities. At the same time, the Barcol hardness increases from 44.2 for the unfilled composite to 54.3 at 0.8 wt% CNF, which is an improvement of roughly 22.9 %. An increase in surface hardness limits the depth of penetration of the abrasive asperities and hence the micro-cutting, ploughing and plastic deformation of the PPS matrix.

The enhanced interlaminar shear strength also implies a better load transmission across the fiber-matrix interface and hence a lower probability of fiber pull-out and delamination during wear. Hence, the composite containing 0.8 wt% CNF exhibited the most balanced structure and the best tribological response, with smoother worn surfaces, shallower grooves, less debris production and lower wear loss. However, at 1 wt% CNF, the agglomeration of nanoparticles and the higher melt viscosity during processing may create voids and localized defects that lead to a decrease in interfacial efficiency and mechanical performance. The results confirm that optimum CNF loading improves wear performance significantly by improving simultaneously microstructure, hardness and interfacial strength.

4. CONCLUSION

The key experimental results, quantitative improvement, and tribological behavior of CNF-reinforced GF/PPS hybrid nanocomposites are summarized in the following conclusions.

- Hybrid GF/PPS composites with 0–1 wt% CNFs were successfully synthesized by melt processing, and FESEM measurements showed that the addition of CNFs significantly improved fiber–matrix interface adhesion and microstructural homogeneity compared with the unfilled composite.
- The density and void-content data revealed that the optimum CNF loading was 0.6–0.8 wt% because of the increased packing effectiveness and lower porosity. On the other hand, 1 wt% CNF addition produced agglomeration of nanoparticles and increased void formation, demonstrating that too much filler addition is deleterious to the quality of the composites.
- The inclusion of CNFs caused a progressive rise in surface hardness because of their high stiffness and reinforcing action. The composite with 0.8 wt% CNF had the highest hardness which was improved by about 12–18% compared to the baseline GF/PPS composites.

- ANOVA analysis revealed that the most important factors influencing wear loss under three-body abrasive wear circumstances were CNF loading and applied load, whereas abrading distance had a relatively less influence.
- Under the same testing conditions, the 0.8 wt% CNF composite had the highest wear resistance of all the compositions, with wear loss decreased by almost 25–35% as compared to the baseline GF/PPS. Higher hardness, effective load transmission, and inhibition of crack development are responsible for this improvement.
- The wear process clearly changed from severe micro-cutting, matrix removal, and fiber debonding in baseline composites to mild micro-ploughing and the creation of compact protective debris layers in CNF-reinforced systems, conferring to SEM characterization of worn surfaces.
- The developed response surface regression model accurately predicted wear loss within the tested parameter window with prediction errors of less than 5%, indicating its suitability for process improvement and performance forecasting.
- For lightweight, wear-resistant components in automotive, aerospace, and industrial applications, CNF-filled GF/PPS hybrid nanocomposites with 0.8 wt% CNF are generally good choices. Long-term performance, large-scale production, and thermal aging may be the main topics of future research.

REFERENCES

[1] H. Rajashekaraiah, S. Bheemappa, S.-H. Yang, and S. Mohan, "Abrasive wear behaviour of thermoplastic copolyester elastomer composites: A statistical approach," *International Journal of Precision Engineering and Manufacturing*, vol. 17, no. 6, pp. 755–763, Jun. 2016, doi: 10.1007/s12541-016-0093-x.

[2] M. M. Y. Zaghloul, K. Steel, M. Veidt, D. Martin, M. Firouzi, and M. T. Heitzmann, "Influence of Counter-Face Grit Size and Lubricant on the Abrasive Wear Behaviour of Thermoplastic Polymers Reinforced with Glass Fibres," *Tribology Letters*, vol. 71, no. 3, Aug. 2023, doi: 10.1007/s11249-023-01774-9.

[3] Y. C. Arun, R. Ravishankar, S. Kumar, M. R. Ramesh, and R. Suresh, "Nanotechnology Perceptions Mechanical Properties Of 3D Printed Carbon Nanofiber Reinforced Polyphenylene Sulfide Composites -A Comprehensive Review," *Nanotechnology Perceptions*, Jan. 2026, doi: 10.13140/rg.2.2.15761.60000.

[4] L. Vaddar et al., "Glass Fiber-Epoxy Composites with Carbon Nanotube Fillers for Enhancing Properties in Structure Modeling and Analysis Using Artificial Intelligence Technique," *ACS Omega*, vol. 8, no. 26, pp. 23528–23544, Jun. 2023, doi: 10.1021/acsomega.3c01067.

[5] R. I. Trezona, D. N. Allsopp, and I. M. Hutchings, "Transitions between two-body and three-body abrasive wear: influence of test conditions in the microscale abrasive wear test," *Wear*, vol. 225–229, pp. 205–214, Apr. 1999, doi: 10.1016/S0043-1648(98)00358-5.

[6] M. Hutchings, "Tribology: friction and wear of engineering materials," *Materials & Design*, vol. 13, no. 3, p. 187, Jan. 1992, doi: 10.1016/0261-3069(92)90241-9.

[7] X. Xiao, Y. Yin, J. Bao, L. Lu, and X. Feng, "Review on the friction and wear of brake materials," *Advances in Mechanical Engineering*, vol. 8, no. 5, May 2016, doi: 10.1177/1687814016647300.

[8] H. Unal, U. Sen, and A. Mimaroglu, "Abrasive wear behaviour of polymeric materials," *Materials & Design*, vol. 26, no. 8, pp. 705–710, Dec.2004, doi: 10.1016/j.matdes.2004.09.004.

[9] Z. Chen, T. Li, Y. Yang, Y. Zhang, and S. Lai, "The effect of phase structure on the tribological properties of PA66/HDPE blends," *Macromolecular Materials and Engineering*, vol. 289, no. 7, pp. 662–671, Jun. 2004, doi: 10.1002/mame.200300266.

[10] H. Unal and A. Mimaroglu, "Influence of test conditions on the tribological properties of polymers," *Industrial Lubrication and Tribology*, vol. 55, no. 4, pp. 178–183, Jun. 2003, doi: 10.1108/00368790310480362.

[11] P. H. Shipway and N. K. Ngao, "Microscale abrasive wear of polymeric materials," *Wear*, vol. 255, no. 1–6, pp. 742–750, May 2003, doi: 10.1016/s0043-1648(03)00106-6.

[12] V. Pejaković, R. Jisa, and F. Franek, "Abrasion resistance of selected commercially available polymer materials," *Tribologia - Finnish Journal of Tribology*, vol. 33, no. 1, pp. 21–27, Jan. 2015.

[13] Y. Jiang and K. T. Turner, "Thermal and mechanical mechanisms of polymer wear at the nanoscale," *ACS Applied Materials & Interfaces*, vol. 16, no. 37, pp. 50004–50011, Sep. 2024, doi: 10.1021/acsami.4c11933.

[14] X. Qiu, A. Gu, W. Tang, S. Tang, and Z. Yu, "Effect of perfluoropolymers on the Anti-Wear properties of Carbon Fiber/Polyphenylene sulfide composites: a comparative study," *ACS Omega*, vol. 7, no. 44, pp. 40316–40323, Oct. 2022, doi: 10.1021/acsomega.2c05298.

[15] M. Kim, J. Lee, M. Cho, and J. Kim, "Improvement of thermal and abrasion resistance performance of polyphenylene sulfide composite through 3-mercaptopropyl trimethoxysilane treatment of carbon fiber and graphene oxide fillers," *Polymer Testing*, vol. 108, p. 107517, Feb. 2022, doi: 10.1016/j.polymertesting.2022.107517.

[16] S. Sathiyamurthy, S. Saravanakumar, and V. Vinoth, "Enhancing tribological performance of hybrid fiber-reinforced composites through machine learning and response surface methodology," *Journal of Reinforced Plastics and Composites*, vol. 44, no. 21–22, pp. 2306–2324, May 2024, doi: 10.1177/07316844241256421.

[17] S. Srinivas, R. Hemanth, B. Harshavardhan, G. S. Ananthapadmanabha, and B. Suresha, "Effect of surface treated nanofillers on abrasive wear of Carbon Fiber/Polyamide blend composites," *Tribology in Industry*, vol. 46, no. 4, pp. 664–676, Dec.2024, doi: 10.24874/ti.1719.07.24.09.

[18] Y. Şahin, A. Deniz, and F. Şahin, "Investigation of abrasive wear performances of different polyamides by response surface methodology," *Tribology in Industry*, vol. 41, no. 3, pp. 321–329, Sep.2019, doi: 10.24874/ti.2019.41.03.02.

[19] A. Sagbas, F. Kahraman, and U. Esme, "Modeling and predicting abrasive wear behaviour of poly oxy methylenes using response surface methodolgy and neural networks," *Metalurgija*, vol. 48, no. 2, pp. 117-120, 2009.

[20] M. A. Ibrahim, H. Çamur, M. A. Savaş, A. K. Sabo, M. Mustapha, and S. I. Abba, "Hybrid Artificial Intelligence Models with Multi Objective Optimization for Prediction of Tribological Behavior of Polytetrafluoroethylene Matrix Composites," *Applied Sciences*, vol. 12, no. 17, p. 8671,Aug.2022, doi: 10.3390/app12178671.

[21] H. Muhandes, Á. Kalácska, L. Székely, R. Keresztes, and G. Kalácska, "Abrasive Sensitivity of Engineering Polymers and a Bio-Composite under Different Abrasive Conditions," *Materials*, vol. 13, no. 22, p. 5239,Nov. 2020, doi: 10.3390/ma13225239.

[22] M. Kumar, R. Kumar, Y. Tak, R. K. Meena, N. Sharma, and A. Kumar, "Parametric optimization and ranking analysis of hybrid epoxy polymer composites based on mechanical, thermo-mechanical and abrasive wear performance," *High Performance Polymers*, vol. 33, no. 4, pp. 361–382,Sep.2020, doi: 10.1177/0954008320959412.

[23] S. Sardar, S. Dey, and D. Das, "Modelling of tribological responses of composites using integrated ANN-GA technique," *Journal of Composite Materials*, vol. 55, no. 7, pp. 873–896, Sep.2020, doi: 10.1177/0021998320960520.

[24] S. Savaş, N. Gurbanov, and M. Doğan, "Effect of fiber type, fiber content, and compatibilizer on two-body abrasive wear performance of HDPE matrix composites," *Journal of Composite Materials*, vol. 53, no. 19, pp. 2743–2760, Apr. 2019, doi: 10.1177/0021998319839135.

[25] K. Sudarshan Rao, "Taguchi and Regression analysis of abrasive wear behavior of carbon epoxy composite," *Journal of Materials and Engineering*, vol. 1, no. 2, pp. 68–73, Jan. 2023, doi: 10.61552/jme.2023.02.003.

[26] H. D. S. Gowda, Hemaraju, V. G. P. Kumar, B. Suresha, C. R. Rachana, and S. K. Bhat, "Optimizing abrasive wear in sustainable MCC reinforced hemp bamboo epoxy composites for tribological applications," *Scientific Reports*, vol. 16, no. 1, Mar. 2026, doi: 10.1038/s41598-026-43505-9.

[27] T. Ö. Öge, "Enhancement and Machine Learning-Based prediction of tribological properties of PC/PBT/GNPS nanocomposites," *ACS Omega*, vol. 10, no. 22, pp. 23639–23662, May 2025, doi: 10.1021/acsomega.5c02538.

[28] S. Kumar, L. Prasad, V. K. Patel, V. Kumar, A. Kumar, and A. Yadav, "Physico-Mechanical properties and Taguchi optimized abrasive wear of alkali treated and fly ash reinforced Himalayan agave fiber polyester composite," *Journal of Natural Fibers*, vol. 19, no. 14, pp. 9269–9282, Oct, 2021, doi: 10.1080/15440478.2021.1982818.

[29] D. K. Jesthi and R. K. Nayak, "Influence of glass/carbon fiber stacking sequence on mechanical and three-body abrasive wear resistance of hybrid composites," *Materials Research Express*, vol. 7, no. 1, p. 015106, Jan. 2020, doi: 10.1088/2053-1591/ab6919.

[30] S. Yan, Y. Tang, G. Bi, B. Xiao, G. He, and Y. Lin, "Optimal Design of Carbon-Based Polymer Nanocomposites Preparation Based on Response Surface Methodology," *Polymers*, vol. 15, no. 6, p. 1494,Mar.2023, doi: 10.3390/polym15061494.

[31] G. R. Chavhan and L. N. Wankhade, "Optimization of Test Parameters that Influence on Dry Sliding Wear Performance of Steel Embedded Glass/Epoxy Hybrid Composites by Using the Taguchi Approach," *Tribology in Industry*, vol. 42, no. 4, pp. 556–571, Dec. 2020, doi: 10.24874/ti.863.03.20.09.

[32] G. Agarwal, A. Patnaik, and R. K. Sharma, "Parametric optimisation of three-body abrasive wear behaviour of long and short carbon fibre reinforced epoxy composites," *Tribology - Materials Surfaces & Interfaces*, vol. 7, no. 3, pp. 150–160,Aug.2013, doi: 10.1179/1751584x13y.0000000040.

[33] U. M. R. Paturi, S. Cheruku, and N. S. Reddy, "The Role of Artificial Neural Networks in Prediction of mechanical and tribological Properties of Composites—A Comprehensive Review," *Archives of Computational Methods in Engineering*, vol. 29, no. 5, pp. 3109–3149, Jan. 2022, doi: 10.1007/s11831-021-09691-7.

[34] M. B. Wakchaure and P. L. Menezes, "Advances in the tribological performance of graphene oxide and its composites," *Materials*, vol. 18, no. 15, p. 3587,Jul.2025, doi: 10.3390/ma18153587.

[35] M. Singh, S. Dodla, R. K. Gautam, and V. Chauhan, "Enhancement of mechanical and tribological properties in glass fiber-reinforced polymer composites with multi-walled carbon nanotubes and ANN-based COF prediction," *Composite Interfaces*, vol. 32, no. 4, pp. 439–459, Oct. 2024, doi: 10.1080/09276440.2024.2417164.

[36] ASTM International, *Standard Test Method for Density, Relative Density, and API Gravity of Liquids by Digital Density Meter*, ASTM Standard D792-20, West Conshohocken, PA, USA: ASTM International, 2020, doi: 10.1520/d0792-20.

[37] ASTM International, *Standard Test Method for Short-Beam Strength of Polymer Matrix Composite Materials and Their Laminates*, ASTM D2344/D2344M-22, West Conshohocken, PA, USA: ASTM International, 2022, doi: 10.1520/d2344_d2344m-22.

[38] ASTM International, *Standard Test Method for Indentation Hardness of Rigid Plastics by Means of a Barcol Impressor*, ASTM D2583-13a, West Conshohocken, PA, USA: ASTM International, 2013, doi: 10.1520/d2583-13a.

[39] ASTM International, *Standard Test Method for Measuring Abrasion Using the Dry Sand/Rubber Wheel Apparatus, ASTM G65-16(R2021)*, West Conshohocken, PA, USA: ASTM International, 2021, doi: 10.1520/g0065-16r21.

[40] R. F. Gunst, R. H. Myers, and D. C. Montgomery, "Response Surface Methodology: process and product optimization using designed experiments," *Technometrics*, vol. 38, no. 3, p. 285, Aug.1996, doi: 10.2307/1270613.

[41] N. Szpisják-Gulyás, A. N. Al-Tayawi, Zs. H. Horváth, Zs. László, Sz. Kertész, and C. Hodúr, "Methods for experimental design, central composite design and the Box–Behnken design, to optimise operational parameters: A review," *Acta Alimentaria*, vol. 52, no. 4, pp. 521–537, Nov. 2023, doi: 10.1556/066.2023.00235.

[42] N. Jagadeesan et al., "Response Surface methodology-based optimization of test parameter in glass fiber reinforced polyamide 66 for dry sliding, tribological performance," *Materials*, vol. 15, no. 19, p. 6520, Sep. 2022, doi: 10.3390/ma15196520.

[43] E. T. Thostenson, Z. Ren, and T.-W. Chou, "Advances in the science and technology of carbon nanotubes and their composites: a review," *Composites Science and Technology*, vol. 61, no. 13, pp. 1899–1912,Oct.2001, 10.1016/S0266-3538(01)00094-X.

[44] J. K. Kim and Y. W. Mai, Eds., *Engineered Interfaces in Fiber Reinforced Composites*. Oxford, U.K.: Elsevier Science Ltd., 1998. 10.1016/S1369-7021(99)80035-2.

[45] F. H. Gojny, M. H. G. Wichmann, U. Köpke, B. Fiedler, and K. Schulte, "Carbon nanotube-reinforced epoxy-composites: enhanced stiffness and fracture toughness at low nanotube content," *Composites Science and Technology*, vol. 64, no. 15, pp. 2363–2371, May 2004, doi: 10.1016/j.compscitech.2004.04.002.

[46] P. M. Ajayan, L. S. Schadler, and P. Braun V., *Nanocomposite Science and Technology*. Wiley, 2003. doi: 10.1002/3527602127.

[47] D. Gay, *Composite materials*. Taylor & Francis, 2022. doi: 10.1201/9781003195788.

[48] P. K. Mallick, *Fiber-reinforced composites: materials, manufacturing, and design*. Taylor & Francis, 2008. doi: 10.1201/9781420005981.

[49] S. Kumar, H. Doshi, M. Srinivasarao, J. O. Park, and D. A. Schiraldi, "Fibers from polypropylene/nano carbon fiber composites," *Polymer*, vol. 43, no. 5, pp.1701–1703,Mar.2002, 10.1016/S0032-3861(01)00744-3.

[50] S. Kirmse, B. Ranabhat, and K.-T. Hsiao, "Experimental and analytical investigation on the interlaminar shear strength of carbon fiber composites reinforced with carbon nanofiber z-threads," *Materials Today Communications*, vol. 25, p. 101512, Aug. 2020, doi: 10.1016/j.mtcomm.2020.101512.

[51] P. Santos, A. P. Silva, and P. N. B. Reis, "Effect of carbon nanofibers on the strain rate and interlaminar shear strength of Carbon/Epoxy composites," *Materials*, vol. 16, no. 12, p. 4332, Jun. 2023, doi: 10.3390/ma16124332.

[52] M. R. Tejas, B. Suresha, C. P. Meghavath, S. Afiya, and A. B. Hemavathi, "Experimental analysis on mechanical properties and three-body abrasive wear behavior of microcrystalline cellulose filled natural fiber composites," *Journal of Composite Materials*, Mar. 2026, doi: 10.1177/00219983261432448.

[53] S. J. D. Hans, M. Muthukumaran, K. Kumaresan, V. G. P. Kumar, D. M. Goudar, and S. K. Bhat, "Hybrid experimental and machine learning approach for optimizing abrasive wear of microcrystalline cellulose modified hemp/bamboo fiber composites," *Scientific Reports*, vol. 15, no. 1, p. 42216, Nov. 2025, doi: 10.1038/s41598-025-26396-0.

[54] M. Kozak and H.-P. Piepho, "What's normal anyway? Residual plots are more telling than significance tests when checking ANOVA assumptions," *Journal of Agronomy and Crop Science*, vol. 204, no. 1, pp. 86–98, 2018, doi: 10.1111/jac.12220.